CHAPTER IV

RESULTS AND DISCUSSION

4.1 Direct Oxidation of Stainless Steel Disks

Several research groups have reported that, at high temperatures, metal components of stainless steel diffused up and formed an oxide film covering the surface [25]. However, none has ever concerned about how such a film can be used as the protective barrier to intermetallic diffusion. In this regard, although iron is far more present in stainless steel, pure Cr_2O_3 film is more suitable for this function than Fe_2O_3 film due to its much higher melting temperature, i.e. 2435°C versus 1565°C.

In order to successfully develop a Cr_2O_3 protective film through direct thermal oxidation of the stainless steel, a clear picture of how much each metal will diffuse at a particular condition is the first thing to be established. The ideal condition for direct thermal oxidation of the stainless steel support to form Cr_2O_3 film should permit:

(1) The highest diffusion of chromium while keep the diffusion of iron and nickel at minimum, and
(2) The formation of the most stable chromium oxide, the Cr_2O_3.

XPS was employed to examine the degree of diffusion and by varying the time of incubation some clues to further optimize the condition were revealed.

4.1.1 Oxidation at 450°C

Greeff *et al.* [22] prepared oxide film of metal alloy FeCrMo and found that FeO and Cr_2O_3 were present only at temperature higher than 400°C otherwise all oxides were Fe_2O_3. The normal 316L stainless steel used in this study is an FeCrNi alloy having comparable metal percentages to those of the FeCrMo therefore in this study the stainless steel disks were oxidized at 450°C. Metal content in the oxide layer after heating at 450°C and the corresponding XPS spectrum of each metal were shown in Table and Figure 4.1, respectively.

Table 4.1 Metal contents in the oxide layer at the stainless steel surface after heating at 450°C

Heating time (hr)	Percentage of metal*		Ratio of metal to oxygen
4	Cr	1.5417	0.017269
	Fe	9.1828	0.102859
	O	89.2754	
6	Cr	17.4273	0.228045
	Fe	1.8654	0.02441
	Ni	4.2867	0.05609
	O	76.4204	
8	Cr	11.4900	0.142487
	Fe	7.8710	0.097608
	O	80.6389	

*as determined by XPS.

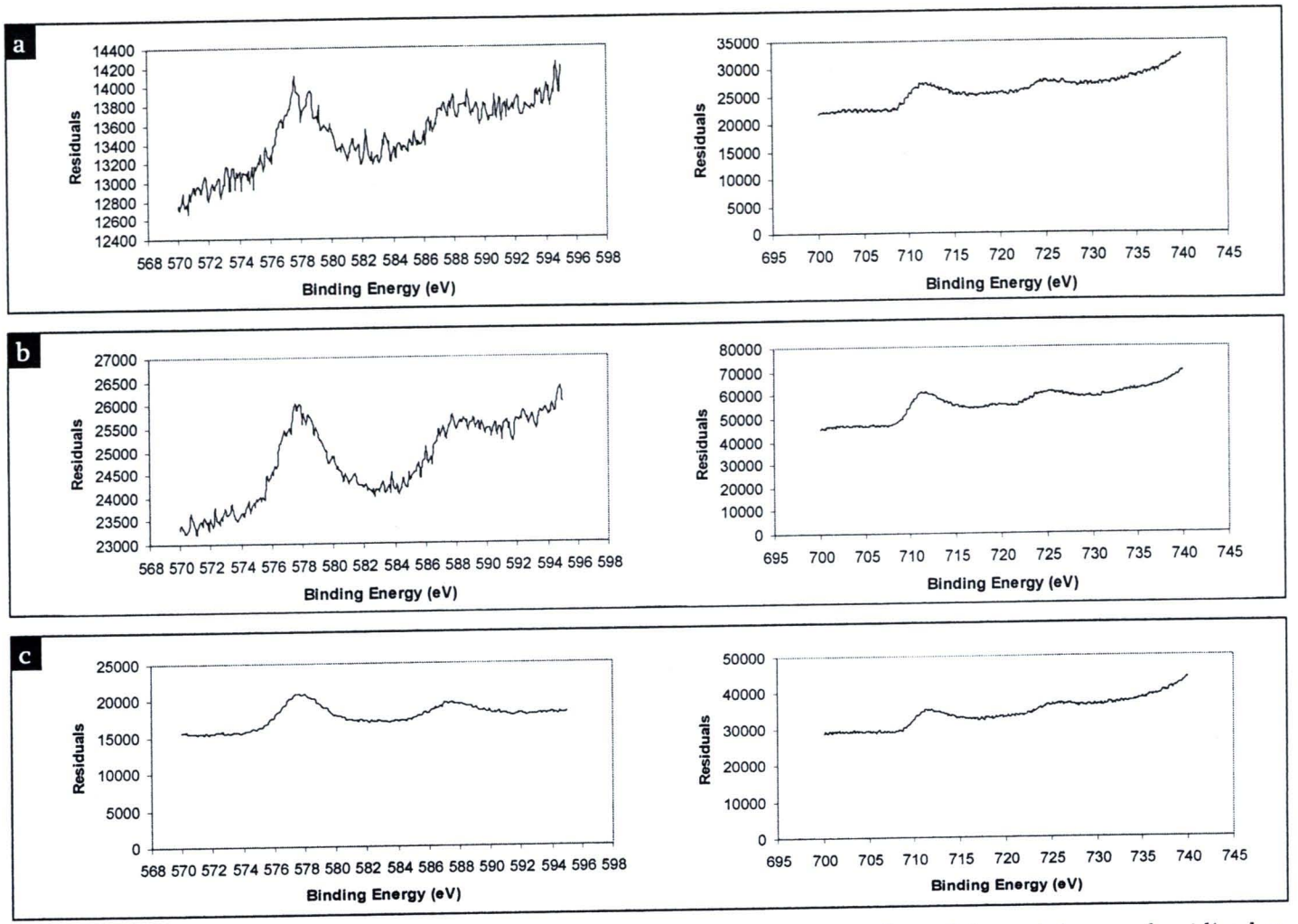

Figure 4.1 XPS spectra of oxides of Cr (left side) and Fe (right side) at the surface of the stainless steel oxidized at 450°C for 4 hr (a), 6 hr (b) and 8 hr (c).

By heating at 450°C for 4 hr, the stainless steel disk became dark and brownish green in colour. Far more iron was oxidized to form a coated film than chromium while, at 6 hr of incubation, the situation was reversed and significant amount of Ni was detected. From 6 to 8 hr of incubation, the diffusion was changed in the opposite direction: accumulation rate of iron oxides began to increase after it first dropped from 4 to 6 hr and no Ni was detected.

These observations can be explained in term of two factors:

(1) The degrees of readiness of metal to diffusion, i.e. how fast each metal diffused at a particular temperature, and
(2) The amount of metal present in the stainless steel, i.e. more percentage means more available for diffusion assuming all metals are evenly distributed.

At 4 hr, the latter factor ruled, that is even though Cr diffusion is faster it cannot compete against Fe that is far more present. This phenomenon was similar to that reported by Greeff *et al.* [22]. Prolonged heating, however, enabled the higher readiness to diffusion of Cr to compensate for its smaller amount. Therefore, in the course of time oxides of Cr outnumbered. At 8 hr, the result seemed to contradict with this explanation, that is percentage of Cr should be even more if the above explanation is correct. But with the fact that Cr is present in smaller amount in the stainless steel, the observation at 8 hr is nothing odd: most of Cr atoms near the surface diffused up and thus longer incubation time leads to the more and more accumulation of iron.

As far as the stability of oxide of Cr is solely concerned, intermetallic diffusion barrier is better prepared at 8 hr of incubation. This is obvious from the left XPS spectra in Figure 4.1. The Cr XPS spectrum of pure Cr_2O_3 as given in Figure A-1 is smooth and has two characteristic peaks at binding energies 577 and 587 eV. The presence of other chromium oxide impurities will be evident as noises resulting in spiky Cr XPS spectra as those observed at 4 or 6 hr. At 8 hr of incubation, however, the Cr XPS spectrum was almost free of noise and its peaks were the characteristics of Cr_2O_3.

4.1.2 Oxidation at 800°C

Ma *et al.* [25] prepared oxide film on porous stainless steel by direct oxidation at 800°C and found that the palladium layer was protected from diffusion at some degrees by the film. However, the form of chromium oxides in the film was not characterized in this study. Therefore, another set of stainless steel disks were heated at 800°C and the results were compared to those obtained at 450°C to establish how metal diffusion changed with temperature. Metal contents in the oxide layer after heating at 800°C and their corresponding XPS spectra were shown in Table and Figure 4.2, respectively.

Table 4.2 Metal contents in the oxide layer at the stainless steel surface after heating at 800°C

Heating time (hr)	Percentage of metal*		Ratio of metal to oxygen
4	Cr	21.70	0.318
	Fe	10.09	0.147
	O	68.19	
6	Cr	16.93	0.178
	Fe	8.47	0.089
	O	74.59	
8	Cr	11.13	0.158
	Fe	18.71	0.266
	O	70.15	
12	Cr	7.93	0.104
	Fe	16.21	0.213
	O	75.84	

*as determined by XPS.

The data from table 4.2 shown, when provided the stainless steel heating at and varied duration time for 4, 6 ,8 and 12 hr, the percentage of metal diffusion into palladium layer gave the same trend with 450°C for heating. The XPS spectra in Figure 4.2 shown, when heating the stainless steel at 800°C that gave the smooth characteristic peak in this reasonable, the temperature for heating at 800°C could prepared the stable chromium Oxide layer but the XPS spectra peak position were incorrect (not appear at 577 and 587 eV) that occur when heating stainless steel 800°C could made other chromium oxide layer didn't Cr_2O_3 form. All of duration times, the percentage of iron atoms were increase higher than 450 °C and the Fe percent in palladium layer so high then 800°C heating temperature was not the appropriate temperature for oxidized stainless steel to made stable chromium oxide layer. Considered the duration times, when heating the stainless steel for 6 hr that shown the iron percentage in palladium layer so slighter than other duration times. The duration time for oxidized plain of stainless steel at 450°C and 800°C gave the same trend, 6 hr for oxidized stainless steel was an appropriate time for established the Cr_2O_3 layer.

With regard to the forms of chromium oxides, none of the incubation time fulfilled the second requirement. Although the Cr XPS spectra at 4, 6 or 8 hr were free of noise as opposed to the spiky spectrum at 12 hr, their peaks were the characteristics of CrO not the Cr_2O_3. The peaks appeared at binding energies 576 and 586 eV instead of 577 and 587 eV. This observation agreed with that of Greeff *et al.* [22] who characterized the oxide film formed at the surface of stainless steel via oxidation at temperatures higher than 700°C and reported that more Cr were in the form of CrO than Cr_2O_3.

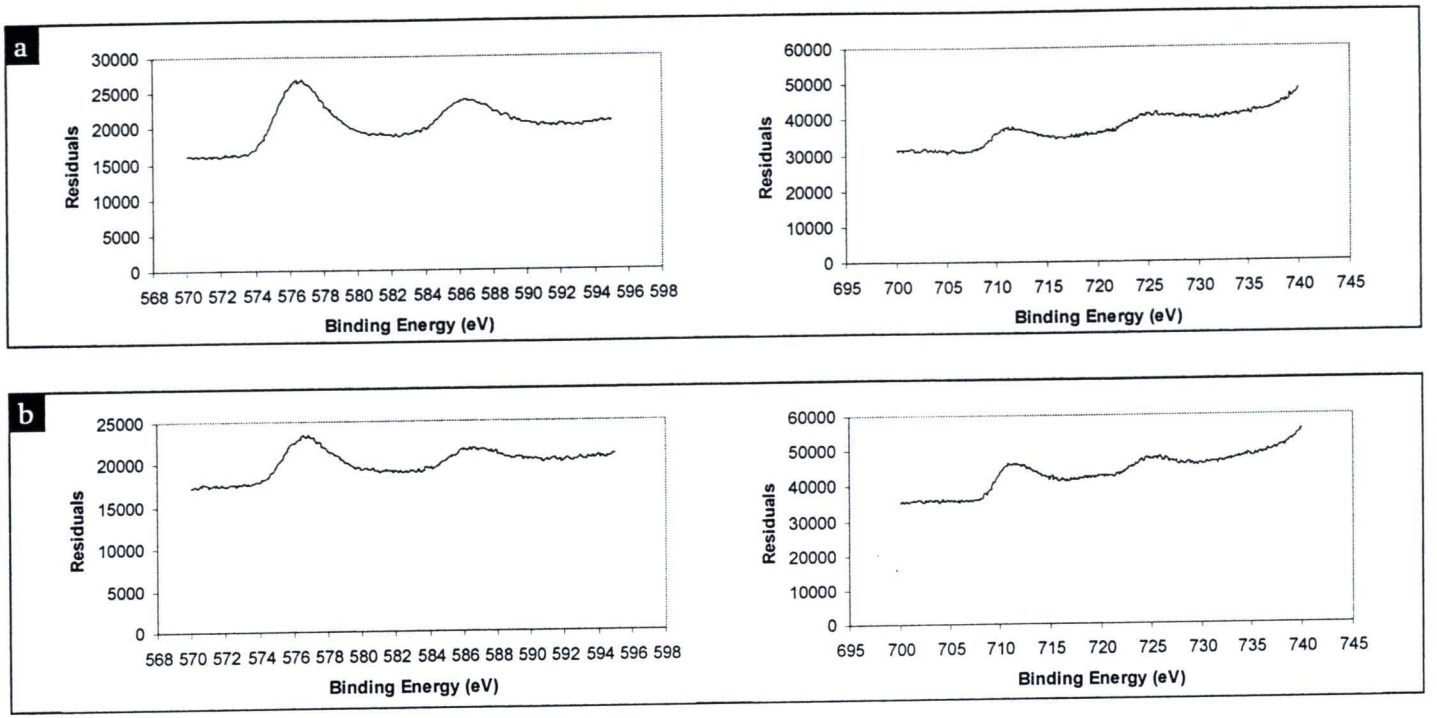

Figure 4.2 XPS spectra of oxides of Cr(left side) and Fe (right side) at the surface of the stainless steel oxidized at 800°C for 4 hr (a) and 6 hr (b).

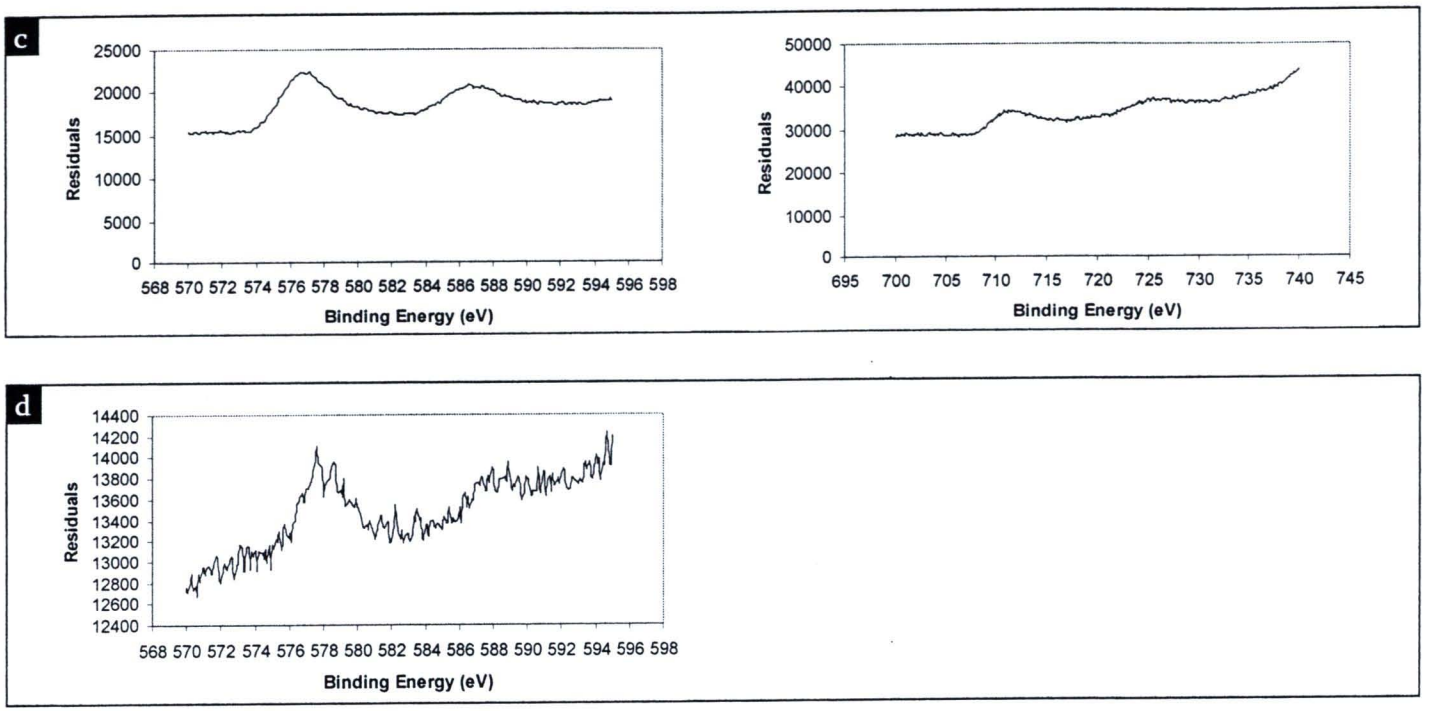

Figure 4.2 (continued) XPS spectra of oxides of Cr (left side) and Fe (right side) at the surface of the stainless steel oxidized at 800°C for 8 hr (c) and 12 hr (d).

4.1.3 Oxidation at 600°C for 6 hr

From the study at 800°C, it is obvious that, in the range of incubation times examined, heating stainless steel at 800°C was not suitable for preparing stable chromium oxide film. When compare with the study at 450°C, it turns out that 800°C was too high. Heating at 450°C was better but there was no incubation time that fulfilled both requirements. The situation got even worse: since the best incubation time for one requirement was on the worse side for the other requirement, choosing one and leave the other will cost very much. In other condition, there must be combined the suitable incubation time and stable Cr_2O_3 film XPS spectra from both of heating temperature. Because of when heating the stainless steel at low and high temperature (450°, 800°C) could not get the suitable Cr_2O_3 film and the stable Chromium oxide film were synthesis at temperature between 450°C and 800°C then would choused 6 hr as a duration time because of the results from table 4.1, 4.2 and Figure 4.1, 4.2. There are two incubation times to choose from: 6 hr at which the highest Cr content was observed or 8 hr at which the highest Cr_2O_3 content was observed. By recalling that Cr_2O_3 was formed at temperature higher than 400°C [22], only the former choice is possible since choosing 8 hr means lowering heating temperature.

By using 450 and 800°C as the lower and upper temperature limits, the temperature that is exactly in the middle is 625°C. If higher temperature is employed to shift the time for the highest Cr_2O_3 content at 8 to 6 hr, the time for the highest Cr content will be shifted in the same direction as well. Therefore, 600°C was chosen in favour of the lower limit. The stainless steel disk was incubated at 600°C for 6 hr and the XPS results were compared to those at 450 and 800°C in Table and Figure 4.3.

Table 4.3 Comparison of metal contents in the oxide layer at the stainless steel surface after heating at 450, 600 or 800°C.

Metal	Temperature	Percentage of metal*	Ratio of metal to oxygen
Cr	450°C	17.42	0.228
	600°C	15.17	0.195
	800°C	16.93	0.178
Fe	450°C	1.86	0.024
	600°C	7.10	0.091
	800°C	8.47	0.089
Ni	450°C	4.28	0.056
	600°C	-	-
	800°C	-	-
O	450°C	76.42	
	600°C	77.72	
	800°C	74.59	

*as determined by XPS.

As expected, incubation at 600°C fine-tuned the performance of thermal oxidation. At 600°C, the Cr XPS spectrum shifted from the characteristic peaks of CrO observed at 800°C to those of Cr_2O_3 observed at 450°C, i.e from binding energies 576 and 586 eV to 577 and 587 eV. Unlike at 450°C for 6 hr, the Cr XPS spectrum at 600°C was almost free of noise and essentially the same as at 450°C, 8 hr. Although the percentage of Cr was not the highest, the two requirements were better compromised at 600°C.

Therefore, 600°C, 6 hr was the condition of choice used throughout in further experiments.

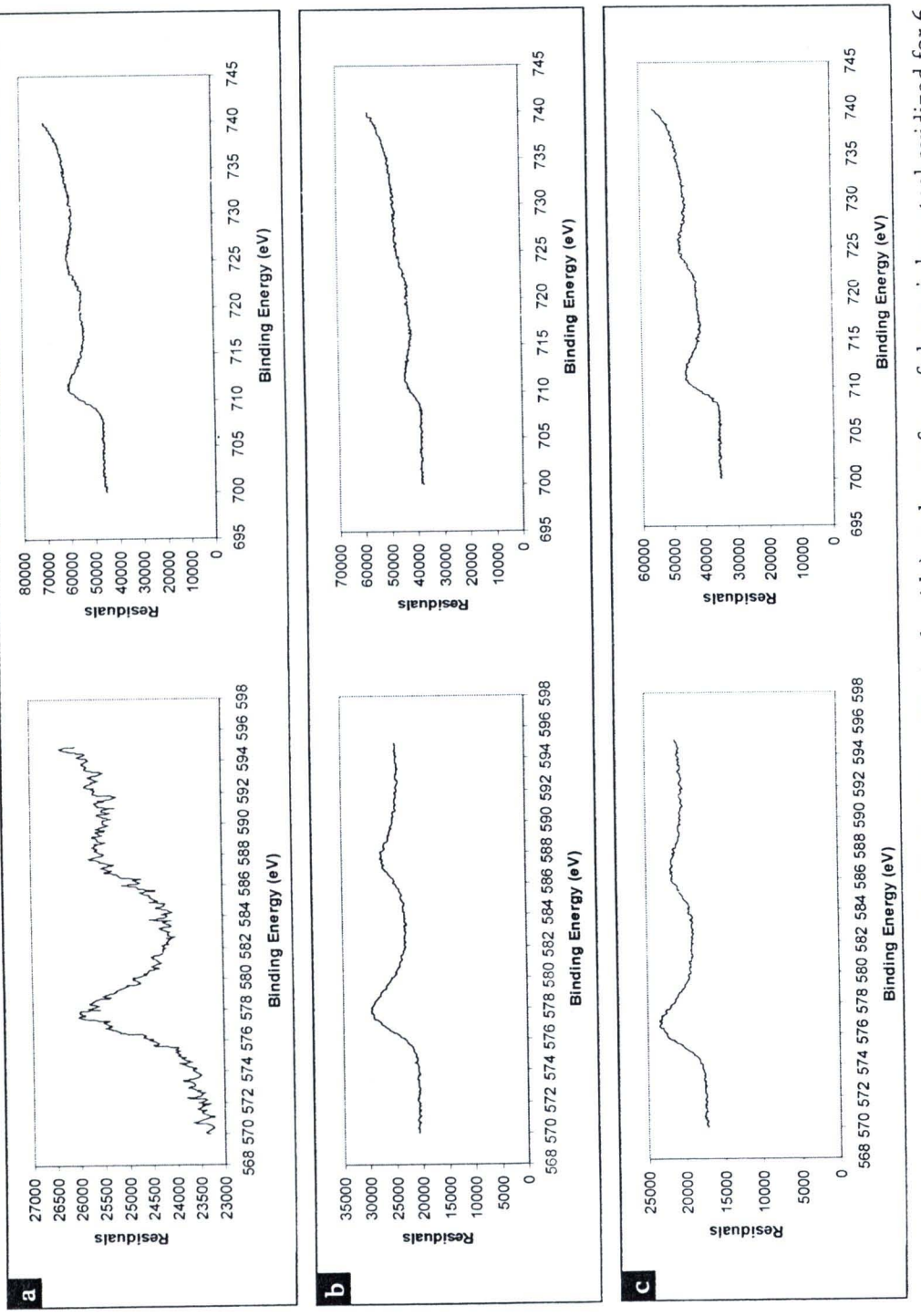

Figure 4.3 XPS spectra of oxides of Cr (left side) and Fe (right side) at the surface of the stainless steel oxidized for 6 hr at (a) 450, (b) 600 and (c) 800°C.

4.2 Cr-Based Intermetallic Diffusion Barriers

4.2.1 Cr_2O_3 intermetallic diffusion barriers

4.2.1.1 Preparation of Cr_2O_3 layer

There are three factors to be considered in preparation of thin film of Cr_2O_3:
(1) Source of Cr,
(2) How to coat Cr on the support, and
(3) How to effectively convert Cr to Cr_2O_3.

With regard to the source of Cr, there are two: internal (Cr inherently in the stainless steel) and external. The external Cr atoms can be coated on the stainless steel support by either (1) electroplating or (2) sputtering. In electroplating, Cr ion was reduced to metal Cr by electrical current and allowed to deposit at the surface of the stainless steel acting as the cathode.

In sputtering, Cr metal was turned to plasma by bombarding with negatively charged particles, the plasma then react with other molecule present in the sputtering chamber, if not inert, forming compound and deposits on the stainless steel substrate. If no reaction occurs, Cr plasma deposits as such forming Cr layer. Reactive Cr-sputtering in oxygen atmosphere is not possible in term of operation setting.

Cr layer prepared by either electroplating or sputtering can be oxidized in a separate step to form Cr_2O_3. Effective oxidation of Cr layer, i.e. throughout its entire thickness, was only possible with a thermal process.

Three methods were employed in this study to prepare Cr_2O_3 intermetallic diffusion barriers on stainless steel.

(1) Direct oxidation of the stainless steel. Since the most abundant metal in stainless steel normal 316L aside from iron itself is Cr which readily diffuses to the surface upon heating, Cr_2O_3 film can be directly formed by thermal oxidation in oxygen atmosphere.

(2) Cr-electroplating/oxidation. The Cr atoms were firstly deposited on the stainless steel support by means of electroplating and then thermally oxidized to form Cr_2O_3 using the same condition as the direct oxidation method.

(3) Cr-sputtering/oxidation. Sputtering of Cr atoms in inert argon atmosphere followed by thermal oxidation using the same condition as the direct oxidation method.

The most effective condition for oxidation of the stainless steel support or the Cr layer to form Cr_2O_3 film was described in section 4.1.

4.2.1.2 Surface characterization of the Cr_2O_3 intermetallic diffusion barriers

SEM micrographs of the surface of the Cr_2O_3 intermetallic diffusion barriers are shown in Figure 4.4. The smooth but grooved surface of the stainless steel (Figure 4.4a) became rough upon thermal oxidation (Figure 4.4b). Fine grains of Cr_2O_3 appeared throughout but the entire surface was not continuously covered by the Cr_2O_3 film as the deep grooves were still there and almost as deep. Within the mass of grains, remnants of the shallow grooves were clearly seen as round dark-grey-to-black spots. Therefore, it is obvious that the stainless steel support provided insufficient amount of Cr and the Cr_2O_3 film was a kind of porous, leaky instead of the intended continuous film.

By contrast, Cr layer produced by electroplating (Figure 4.4c) or sputtering (Figure 4.4e) was continuously formed. No groove previously present on the stainless steel surface was visible even the deepest ones. The surface textures were not changed much after oxidation. Cr_2O_3 grains produced by sputtering/oxidation were extremely fine and the film texture was very smooth as a result (Figure 4.4d). Electroplating/oxidation, on the other hand, produced either very large grains or clumps of Cr_2O_3 (Figure 4.4f). It occurs to everyone that 'how much the uniformity the Cr_2O_3 molecules were deep inside the film?' as this directly affects its protective property.

Another thing worth noted is that although it was carefully selected to minimize Fe/Ni contamination while maximize the formation of Cr_2O_3 (see Section 4.1), the oxidation condition did nothing to ensure that Cr atoms were oxidized throughout its entire thickness. Deeper Cr atoms may not be effectively oxidized in this condition especially those that lied deep in the Cr layer prepared by electroplating which were among the thickest (see Section 4.3 for their cross-section SEM micrographs).

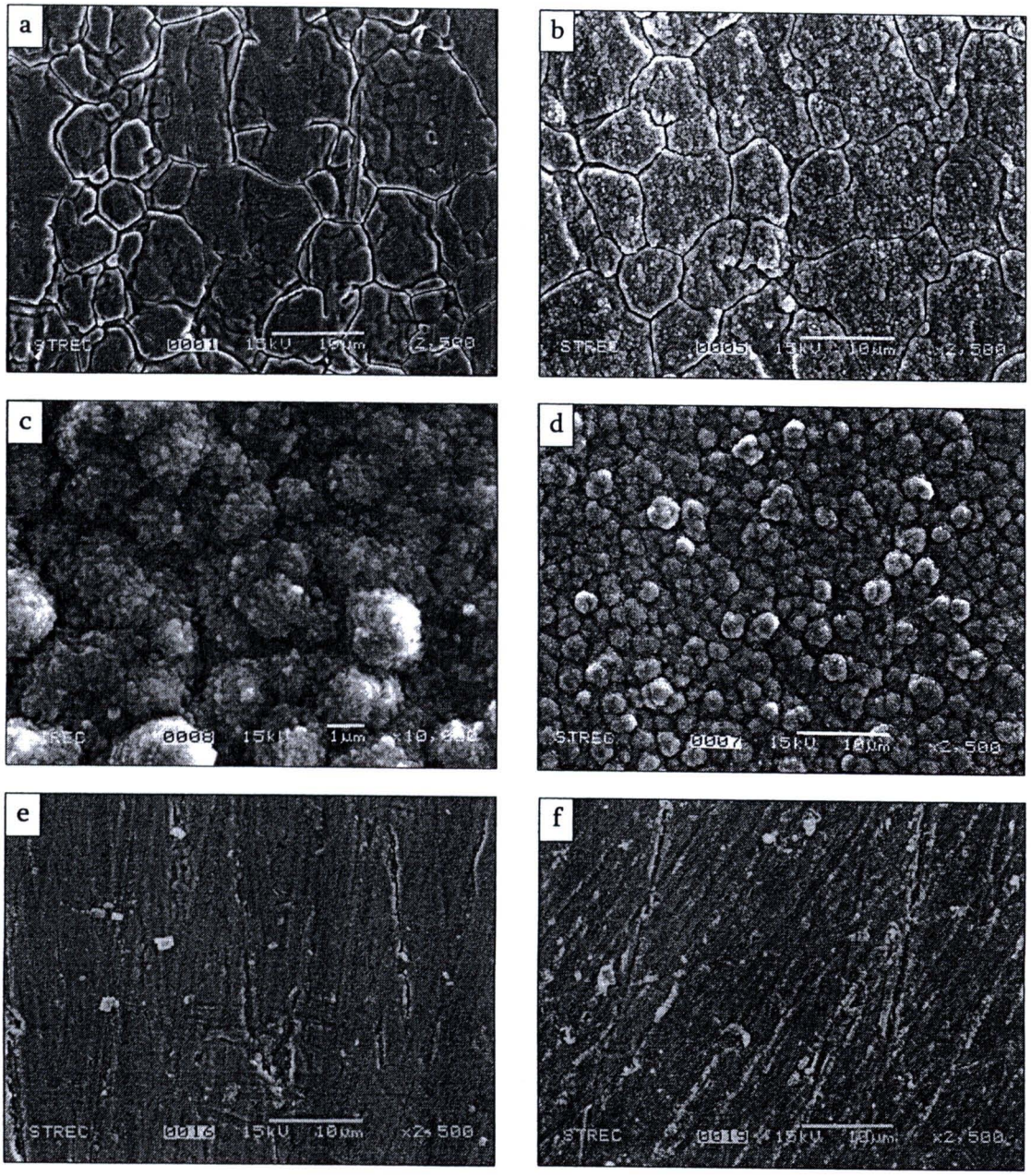

Figure 4.4 SEM micrographs of the stainless steel support with different intermetallic diffusion barriers: **a**: plain and unoxidized stainless steel **b**: Cr_2O_3 barrier by thermal oxidation; **c**: Cr layer by Cr-electroplating; **d**: Cr_2O_3 barrier after oxidation of Cr layer shown in **c**; **e**: Cr layer by Cr-sputtering; **f**: Cr_2O_3 barrier after oxidation of Cr layer shown in **e**.

4.2.2 CrN Intermetallic Diffusion Barrier

The CrN intermetallic diffusion barrier was prepared by Cr-sputtering in nitrogen atmosphere. Nitritation [26], N_2 analogue of thermal oxidation, of the stainless steel or electroplated Cr layer was not possible in term of operation setting.

It is evident when compare the surface of CrN film (Figure 4.5b) with those of Cr_2O_3 films (Figure 4.4) that CrN film prepared at the condition of this study was thicker than Cr_2O_3 film prepared by direct oxidation but thinner than those prepared by oxidized electroplating or sputtering. The surface grooves were filled with CrN. Although the deepest grooves were not completely filled as it was the case with oxidized electroplating or sputtering, it is obvious that the CrN film was a continuous one.

One thing worth mentioned here is that sputtering produced characteristic smooth surfaces (compare Figure 4.5b and 4.4e-f with 4.4b or 4.4c-d) due to the extremely fine grains of Cr or Cr compound formed.

Another issue needs to be focus is that the CrN film produced by sputtering was free from any impurity. XPS analysis revealed that 74.9816% was Cr and the rest 25.0183% was N and XPS spectra given in Figure 4.5c-d indicated that all were in the form of CrN.

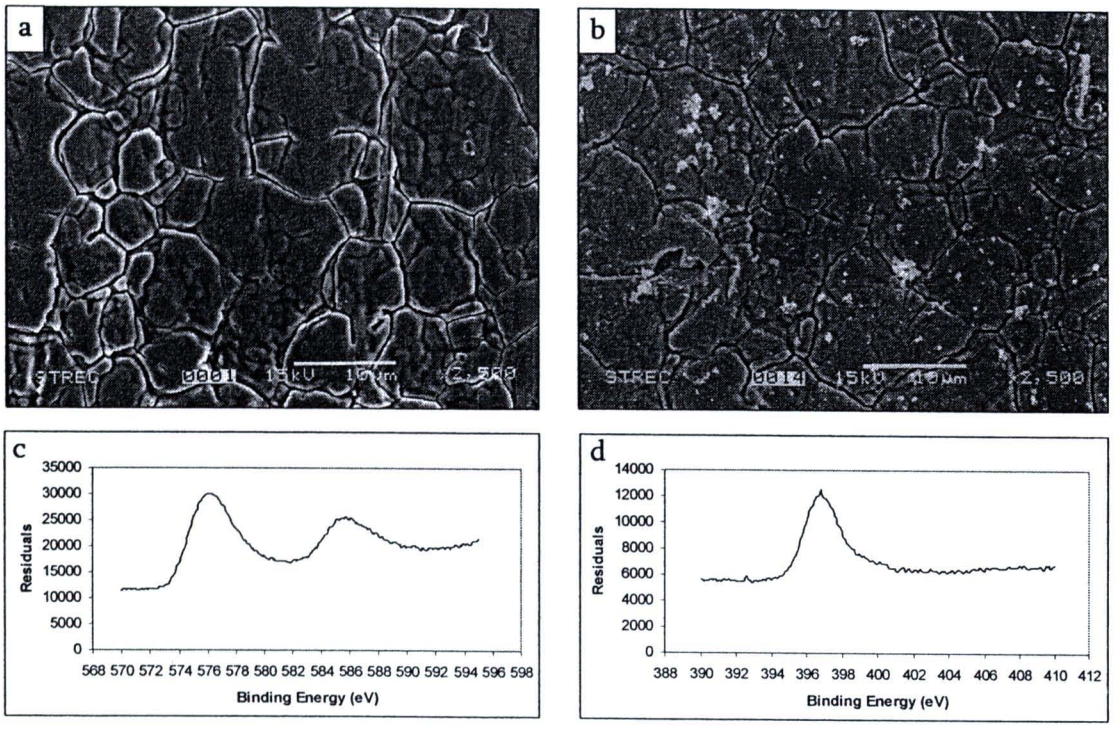

Figure 4.5 Characterization of the CrN intermetallic diffusion barrier. SEM micrographs of the unoxidized stainless steel (a) and the CrN film on the stainless steel support (b). Cr XPS spectrum of the CrN film is shown in (c) while N XPS spectrum is in (d). The characteristic peaks of Cr and N in CrN were at binding energies 376 and 386, and 395 eV, respectively.

4.3 Preparation of Palladium Membrane

The electroless plating technique (Mardilovich *et al.* [27]) was used in preparing the thin film of palladium on the stainless steel. The procedure is composed of 3 important steps: (1) surface cleaning of the support for degreasing, (2) surface activation with $SnCl_2$ and $PdCl_2$ for reducing the plating time, and (3) palladium plating with $Pd(NH_3)_4Cl_2$ solution.

4.3.1 Surface Cleaning

The stainless steel was chosen as a support since it is tougher and stronger and has higher resistance to corrosion than other materials, for example, other grade of stainless steels, ceramic and glass. The stainless steel square disks of 1 x 1 cm^2 in dimension were firstly cleaned with either an alkali solution or commercial solvents. Without this step, the palladium plating could not be deposited successfully because of grease, oil, dirt, corrosion products and others existing on the disk surface.

4.3.2 Surface Activation

Next step was to activate the surface of stainless steel disk in order to initiate an autocatalytic process of the reduction of a metastable salt complex on the target surface during electroless plating [28]. This was performed by the repeated, alternate treatments with $SnCl_2$ and $PdCl_2$ solutions. The SEM micrographs of the stainless steel surface before and after surface activation in Figure 4.6 clearly indicated that the surface was effectively activated. A large number of seeds with relatively uniform particles on the support surface were observed.

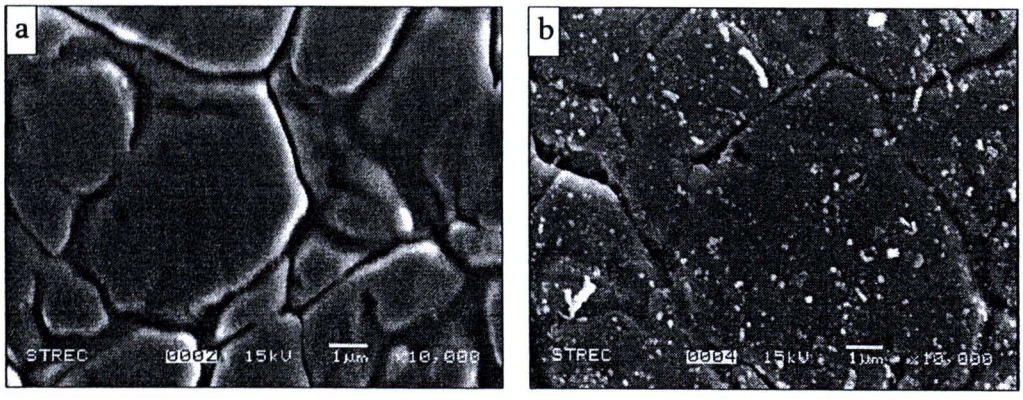

Figure 4.6 SEM micrographs of the stainless steel before (a) and after (b) surface activation.

It was proposed that tin nuclei were firstly created by decomposing of $SnCl_2$ to $Sn(OH)_{1.5}Cl_{0.5}$ with deionized water according to equation 4.1 followed by the deposition of palladium on the tin layer via the redox process described in equation 4.2 [27].

$$2SnCl_2 + 3H_2O \longrightarrow 2Sn(OH)_{1.5}Cl_{0.5} + 3HCl \qquad 4.1$$

$$Pd^{2+} + Sn^{2+} \longrightarrow Pd^0 + Sn^{4+} \qquad 4.2$$

This phenomenon was previously proved by Shu *et al* [29]. They reported that almost no palladium seed appeared on the surface of porous stainless steel disk when it was immersed only in the acidic palladium-containing solution.

4.3.3. Palladium plating

After surface activation, the stainless steel disks were plated with palladium by electroless plating technique. The plating solution consisted of $Pd(NH_3)_4Cl_2{\cdot}H_2O$, 28% ammonia solution, and EDTA. An excess of ammonium hydroxide is necessary to stabilize the plating solution and maintain the pH at 10.

Anhydrous hydrazine, a reducing agent, was then added into the palladium plating solution when its temperature reached 60°C. During the immersion of the disks some bubbling gases were observed due to the redox reaction as shown in Figure 4.7

$N_2H_4 + 4OH^-$	$\longrightarrow$	$4H_2O + N_2 + 4e^-$	$E^0 = -1.12$ V
$2Pd(NH_3)_4^{2+} + 4e^-$	$\longrightarrow$	$2Pd^0 + 8NH_3$	$E^0 = 0.95$ V
$2Pd(NH_3)_4^{2+} + N_2H_4 + 4OH^-$	$\longrightarrow$	$2Pd^0 + 4H_2O + N_2 + 8NH_3$	$E^0 = 2.07$ V

Figure 4.7 Redox reaction of palladium plating

At the end of plating step, the disk was cleaned and dried. It appeared silver-like in color which is the indication that palladium deposition had occurred. It was explained by several other research groups [29, 30] that the reaction occurred on the surface of the support, and preferentially around the palladium seeds. The occurrence was initiated by the reaction of hydrazine with hydroxide ion forming nitrogen gas and water with simultaneous release of electron. The electrons were transferred across the palladium island and used for reducing Pd^{2+} complex into palladium metal. The palladium metal was deposited onto the nuclei resulting in growth. Nitrogen and ammonia gases were concomitantly evolved as bubbles during the plating process.

The palladium plating was evident when compare the SEM micrographs of activated stainless steel disk before and after palladium plating as revealed in Figure 4.8. It obviously showed that the smooth surface was obtained resulting from palladium deposition onto the disk surface until a certain thickness was developed.

In general, the thickness of palladium layer can simply be determined by weighing. Three squares of activated stainless steel disk were weighted before the plating step and then again after palladium plating at different plating time. The calculation for the thickness of palladium layer was done by using the following equation:

$$\text{Pd thickness } (\mu\text{m}) = \left[\left(\frac{\text{plated disk weigh - initial disk weigh}}{\text{disk surface area} \times \text{palladium density}}\right)\right] \times 10^4$$

where density of palladium = 12.02 g/mL, and
surface area = $4(0.1\times1) + 2(1\times1) = 2.4$ cm^2.

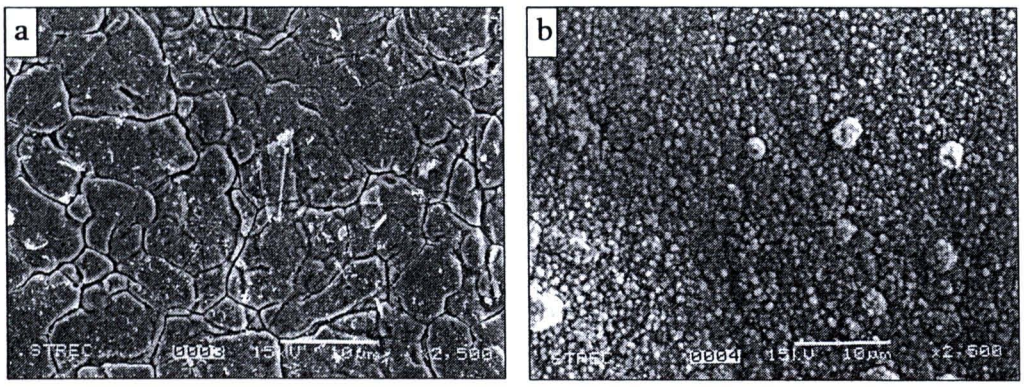

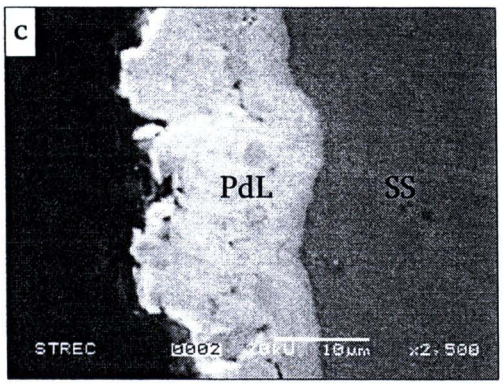

Figure 4.8 SEM micrographs of the activated surface of stainless steel before (a) and after (b) palladium plating. The cross section of (b) is given in (c). PdL: palladium layer; SS: stainless steel.

It was assumed that the gained weight of the disk came from plated palladium only and the entire disk surface was plated evenly. The reliability of the weighing method in determining the palladium layer thickness was assessed with their SEM micrographs. Both measuring methods showed that the palladium layer thickness increased with increasing plating time as illustrated in Table 4.4. It can be seen that the palladium layer thickness measured by weighing is in the range determined by SEM. Therefore, the measurement of palladium layer thickness by weighing could be acceptable.

Table 4.4 Palladium layer thickness on stainless steel disks.

Underlying Surface	Disk number	Disk weight (g)		Pd layer thickness (μm)	
		Before plating	After plating	Weighing	SEM
plain stainless steel	1	1.1825	1.1944	4.1250	4.00
	2	1.1625	1.1742	4.0557	5.16
	3	1.2020	1.2147	4.4023	8.16
Cr_2O_3 by direct oxidation	4	1.0690	1.0745	3.3277	3.50
	5	1.0246	1.0432	6.4775	5.50
	6	1.0360	1.0546	6.4775	4.50
Cr_2O_3 by oxidized Cr-electroplating	7	1.1545	1.1649	3.6051	3.83
	8	1.0103	1.0212	3.7784	3.50
	9	1.2809	1.2984	6.0662	5.16
Cr_2O_3 by oxidized Cr-sputtering	10	1.1716	1.1805	3.0851	3.00
	11	0.8841	0.8913	2.4958	2.83
	12	1.1656	1.1741	2.9464	2.66
CrN	13	1.0968	1.1024	1.9410	2.16
	14	1.0370	1.0464	3.2584	3.16
	15	1.1470	1.1565	3.2931	2.00

4.4 Prevention of Intermetallic Diffusion by Cr-Based Intermetallic Diffusion Barriers.

4.4.1 Effect of high temperature on metal diffusion

The efficacies in preventing intermetallic diffusion [31] of the barriers were assessed by annealing of the palladium membrane with either of the barriers at 450°C, 500°C, and 550°C for 24 hr under argon atmosphere and the elemental composition of the palladium layer were determined by EDS spot (Table 4.5-4.6) of their cross-section and mapped with SEM-EDS (Figure 4.11-16).

When compare among the palladium membrane without any protective barrier, elemental compositions in Table 4.5 clearly demonstrates the intermetallic diffusion of Fe, Cr and Ni from the stainless steel support to the palladium layer. The intermetallic diffusion exhibited the expected trend: diffusion increased with increasing temperatures. However, the degree in which each metal diffuses varied: more Fe and Cr accumulated at the palladium layer than Ni. In this regard, there are two factors to be considered as stated earlier:

(1) The amount of metal present in the stainless steel support, i.e. more metal percentage means more are available to diffuse, and
(2) The nature of the metal, in descending order of readiness, Cr, Fe and Ni.

EDS mapping and EDS spectra of these metals are given in Figures 4.9 and 4.10 for the representative palladium layer on an unoxidized stainless steel.

Table 4.5 Metal distribution in the palladium membrane heated at 450°C

%Metal		No barrier		Cr_2O_3 (1)		Cr_2O_3 (2)		Cr_2O_3 (3)		CrN	
		Mean	SD	Mean	SD	Mean	SD	Mean	SD	Mean	SD
Pd layer	Pd	96.43	0.59	98.72	0.58	99.20	0.26	98.30	0.36	98.72	0.48
	Fe	2.41	0.48	0.71	0.16	0.26	0.12	1.32	0.17	0.87	0.19
	Cr	0.66	0.24	0.26	0.11	0.43	0.14	0.22	0.16	0.53	0.22
	Ni	0.50	0.07	0.31	0.43	0.11	0.20	0.16	0.14	0.07	0.09
Interlayer	Pd	n/d	n/d	n/d	n/d	0.15	0.13	n/d	n/d	n/d	n/d
	Fe	n/d	n/d	n/d	n/d	0.23	0.15	n/d	n/d	n/d	n/d
	Cr	n/d	n/d	n/d	n/d	99.55	0.19	n/d	n/d	n/d	n/d
	Ni	n/d	n/d	n/d	n/d	0.07	0.09	n/d	n/d	n/d	n/d
SS	Pd	0.67	0.91	0.09	0.12	0.00	0.00	0.10	0.08	0.14	0.24
	Fe	70.71	0.43	71.21	0.05	70.54	0.30	71.09	0.42	71.36	0.25
	Cr	18.71	0.70	18.67	0.13	18.59	0.03	18.30	0.04	18.02	0.20
	Ni	9.92	0.21	10.05	0.20	10.88	0.28	10.59	0.16	10.48	0.09

(1): by direct oxidation; (2): by oxidized Cr-electroplating; (3): by oxidized Cr-sputtering; n/d: not determined due to no barrier or too thin barrier to be spotted.

Table 4.5 showed that all forms of intermetallic diffusion barrier can, at varying degrees, prevent the diffusion.

Pair-wise comparisons of the efficacies showed that:

(1) Direct oxidation barriers, oxidized Cr-electroplating, oxidized Cr-sputtering and CrN versus No barrier: The atoms of Cr and Fe in palladium layer were decreased, while atoms of palladium increased.

(2) Oxidized Cr-electroplating versus direct oxidation: The atoms of Fe in palladium layer were decreased but atoms of Cr increased, while atoms of palladium increased. The increasing of Cr atoms may be due to the diffusion of unoxidized Cr atom.

(3) Oxidized Cr-sputtering versus oxidized Cr-electroplating: The atoms of Fe in palladium layer were increased but atoms of Cr decreased, while atoms of palladium decreased. The decreasing of Cr atoms may be due to the lower thickness of sputtering layer.

(4) CrN versus oxidized Cr-sputtering: The atoms of Fe in palladium layer were decreased but atoms of Cr increased, while atoms of palladium increased. The increasing of Cr atoms may be due to the diffusion of unnitrided Cr atom.

Table 4.6 Metal distribution in the palladium membrane heated at 450, 500 and 550°C.

Barriers	% Metal	450°C						500°C						550°C					
		Pd layer		Interlayer		SS		Pd layer		Interlayer		SS		Pd layer		Interlayer		SS	
		Mean	SD	Mean	SD	Mean	SD	Mean	SD	Mean	SD	Mean	SD	Mean	SD	Mean	SD	Mean	SD
No barrier, unoxidized	Pd	96.43	0.59	n/d	n/d	0.67	0.91	87.42	0.55	n/d	n/d	0.05	0.06	73.86	1.62	n/d	n/d	0.01	0.01
	Fe	2.41	0.48	n/d	n/d	70.71	0.43	7.99	0.36	n/d	n/d	70.85	0.39	21.47	1.15	n/d	n/d	71.04	0.91
	Cr	0.66	0.24	n/d	n/d	18.71	0.70	3.70	0.27	n/d	n/d	19.37	0.06	3.45	0.76	n/d	n/d	19.47	0.13
	Ni	0.50	0.07	n/d	n/d	9.92	0.21	0.89	0.18	n/d	n/d	9.74	0.38	1.22	0.26	n/d	n/d	9.49	1.05
Cr2O3 (direct oxidation)	Pd	98.72	0.58	n/d	n/d	0.09	0.12	97.40	0.44	n/d	n/d	0.10	0.11	96.94	0.59	n/d	n/d	0.11	0.01
	Fe	0.71	0.16	n/d	n/d	71.21	0.05	1.73	0.32	n/d	n/d	70.53	0.12	2.16	0.20	n/d	n/d	71.53	0.02
	Cr	0.26	0.11	n/d	n/d	18.67	0.13	0.49	0.17	n/d	n/d	19.39	0.17	0.29	0.21	n/d	n/d	18.61	0.13
	Ni	0.31	0.43	n/d	n/d	10.05	0.20	0.38	0.27	n/d	n/d	9.995	0.03	0.63	0.25	n/d	n/d	9.76	0.15
Cr2O3 (oxidized Cr-electroplating)	Pd	99.20	0.26	0.15	0.13	0.00	0.00	98.80	0.39	0.76	0.44	0.01	0.01	98.36	0.51	0.35	0.04	0.36	0.20
	Fe	0.26	0.12	0.23	0.15	70.54	0.30	0.80	0.27	0.49	0.33	72.02	0.27	1.04	0.34	0.32	0.14	68.82	2.44
	Cr	0.43	0.14	99.55	0.19	18.59	0.03	0.25	0.07	98.59	0.31	16.37	0.78	0.30	0.09	98.40	0.25	20.68	3.64
	Ni	0.11	0.20	0.07	0.09	10.88	0.28	0.17	0.15	0.17	0.25	11.62	0.52	0.30	0.11	0.93	0.08	9.66	0.30
Cr2O3 (oxidized Cr-sputtering)	Pd	98.30	0.36	n/d	n/d	0.10	0.08	98.13	0.28	n/d	n/d	0.16	0.14	98.07	0.56	n/d	n/d	0.18	0.08
	Fe	1.32	0.17	n/d	n/d	71.09	0.42	1.22	0.43	n/d	n/d	71.54	0.17	1.02	0.40	n/d	n/d	70.60	0.18
	Cr	0.22	0.16	n/d	n/d	18.30	0.04	0.50	0.06	n/d	n/d	17.98	0.34	0.68	0.17	n/d	n/d	18.09	0.11
	Ni	0.16	0.14	n/d	n/d	10.59	0.16	0.15	0.13	n/d	n/d	10.32	0.13	0.24	0.19	n/d	n/d	11.13	0.26
CrN	Pd	98.72	0.48	n/d	n/d	0.14	0.24	96.74	0.55	n/d	n/d	0.27	0.24	94.75	2.25	n/d	n/d	0.26	0.24
	Fe	0.87	0.19	n/d	n/d	71.36	0.25	1.82	0.29	n/d	n/d	70.95	0.75	1.76	0.67	n/d	n/d	71.02	0.26
	Cr	0.53	0.22	n/d	n/d	18.02	0.20	0.88	0.09	n/d	n/d	18.15	0.12	2.43	1.07	n/d	n/d	18.32	0.39
	Ni	0.07	0.09	n/d	n/d	10.48	0.09	0.56	0.49	n/d	n/d	10.71	0.32	1.06	1.60	n/d	n/d	10.80	0.22

n/d: not determined due to no barrier or too thin barrier to be spotted.

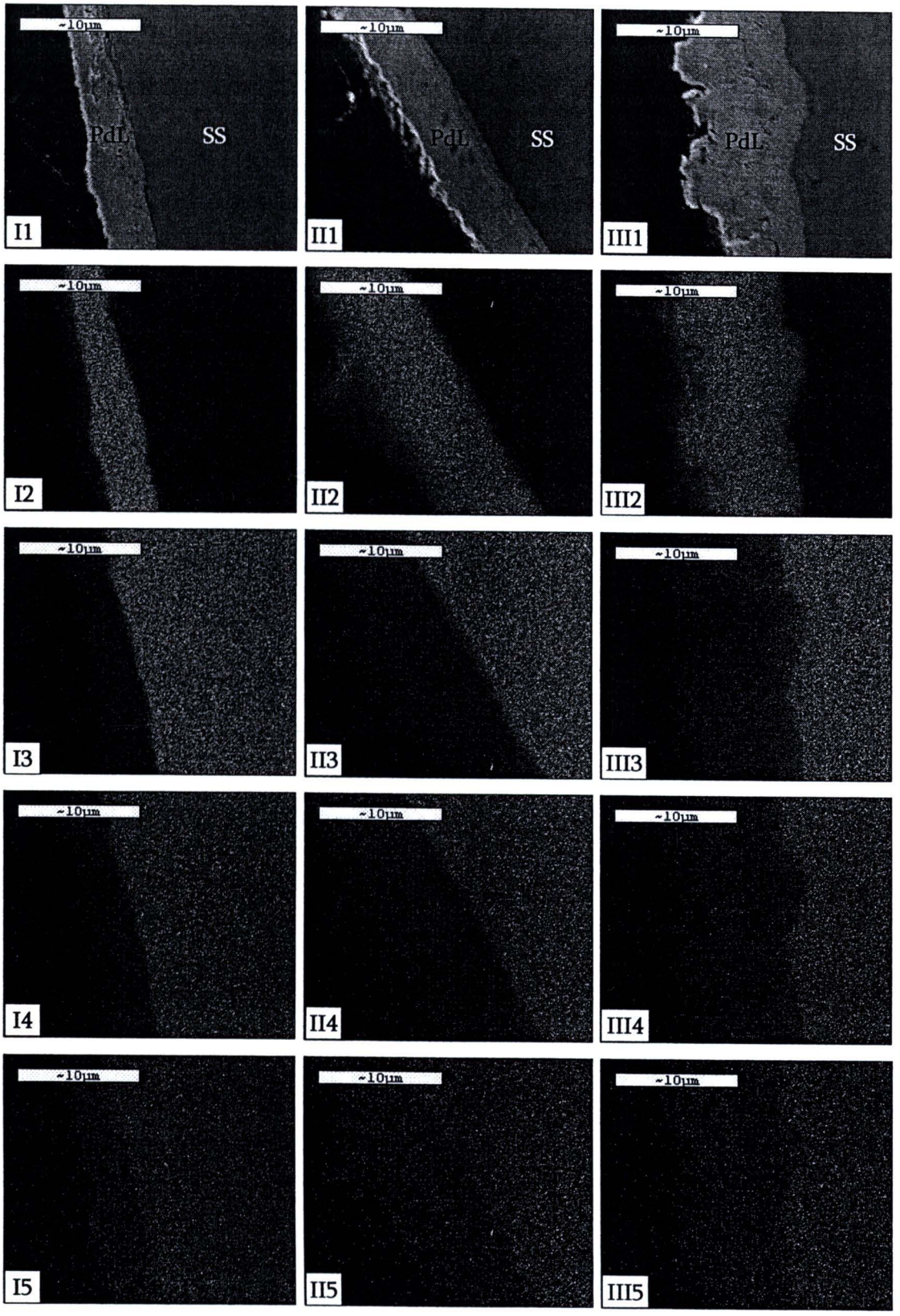

Figure 4.9 SEM micrographs (2500X) of the cross sections of palladium on an unoxidized stainless steel after heating for 24 hr at 450°C (column I, I1-I5), 500°C (column II, II1-II5) or 550°C (column III, III1-III5). Metal distribution were mapped in each row for Pd (row 2, I2-III), Fe (row 3, I3-III3), Cr (row 4, I4-III4) and Ni (row 5, I5-III5). PdL: Pd layer, SS: stainless steel.

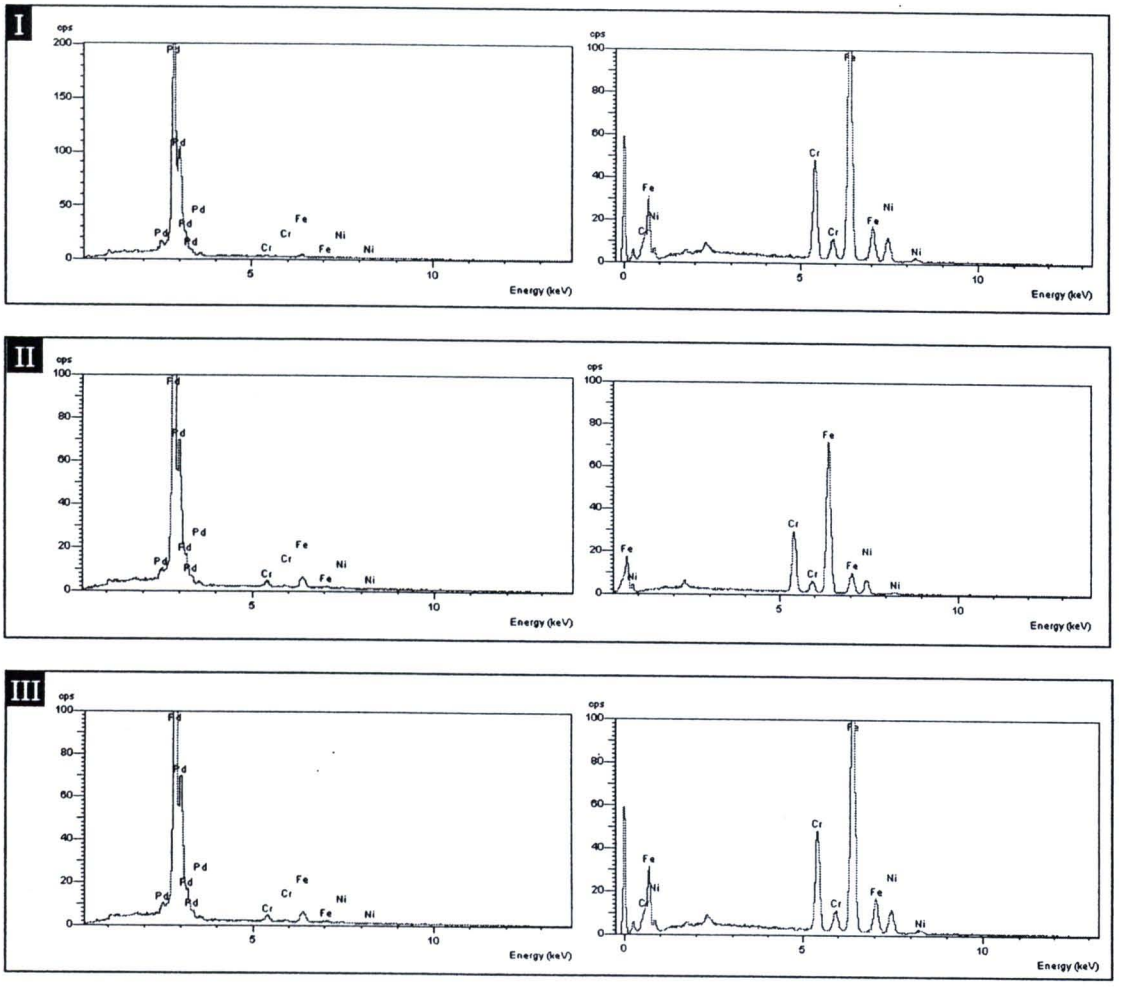

Figure 4.10 EDS spectra of the palladium membrane and unoxidized PSS support after heating for 24 hr at 450°C (I), 500°C (II) or 550°C (III). Shown in I are the EDS spectra of the untreated membrane. EDS spectra of the Pd layer are shown on the left while those of the PSS support are on the right.

4.4.2 Efficacies in preventing intermetallic diffusion

Table 4.6 showed that all forms of intermetallic diffusion barrier can, at varying degrees, prevent the diffusion. Their shielding abilities seem to be independent of temperature at least in the range of conditions tested, i.e. at 450-550°C for 24 hr. Recall that increasing temperature resulted in more diffusion and more accumulation of metal in the palladium layers. Thus, more metal contaminating in the palladium layer observed at higher incubation temperatures does not always means that the efficacy of the barrier was dropped although this is not ruled out. It may merely the result of more metals trying to penetrate the barrier to the palladium layer.

Pair-wise comparisons of the efficacies showed that:

(1) Cr_2O_3 versus CrN barriers: the Cr_2O_3 is a more effective barrier than the CrN probably because Cr_2O_3 is more stable. Even the leaky Cr_2O_3 protective barrier formed via direct oxidation was more effective than the continuous CrN film.

(2) Direct oxidation versus oxidized Cr-electroplating and direct oxidation versus oxidized Cr-sputtering: The Cr_2O_3 barriers prepared by either of the latter method in each pair are more effective than that formed by direct oxidation. The difference in their effectiveness was markedly amplified at higher temperatures. This can be explained in term of amount of Cr available to be oxidized and forms the film. The barrier formed by direct oxidation is too thin to be seen in its cross-section SEM micrograph (A1 and A2 in Figures 4.11, 4.13 and 4.15). It is evident when compare its surface with that of the unoxidized stainless steel (Figure 4.4B versus 4.4A) that the Cr atoms diffused up from the stainless steel were not adequate to form a continuous film to cover the entire surface of the stainless steel.

(3) Oxidized Cr-electroplating versus oxidized Cr-sputtering: The Cr layer was better prepared by electroplating. This is may due to
   (a) The thicker Pd layer (C1 versus D1 in figure 4.11, 4.13 and 4.15) which in turn may be a result of a rough Cr layer (Figure 4.4C versus 4.4D),
   (b) The denser Cr layer formed by chemisorptions versus the physicsorption mechanism of the sputtering.

This study ranks Cr_2O_3 thin film prepared by oxidized Cr-electroplating as the most effective intermetallic diffusion barriers in term of shielding the palladium layer. Cr_2O_3 thin film prepared by oxidized Cr-sputtering comes at the second place followed by the film formed via direct oxidation and the CrN film. However, there is one word of caution: the ranking this study suggested was made without considering of the thickness of the barriers which I found very difficult to manage to get the same. I am pretty sure that Cr_2O_3 film is a better barrier than the CrN as it is obvious from the fact that even the continuous and fairly thick CrN film was outperformed by the leaky and extremely thin Cr_2O_3 film prepared by direct oxidation. But within the group of Cr_2O_3 films, it is by no means certain that there is a significant difference in shielding effectiveness when the films are all equally thick.

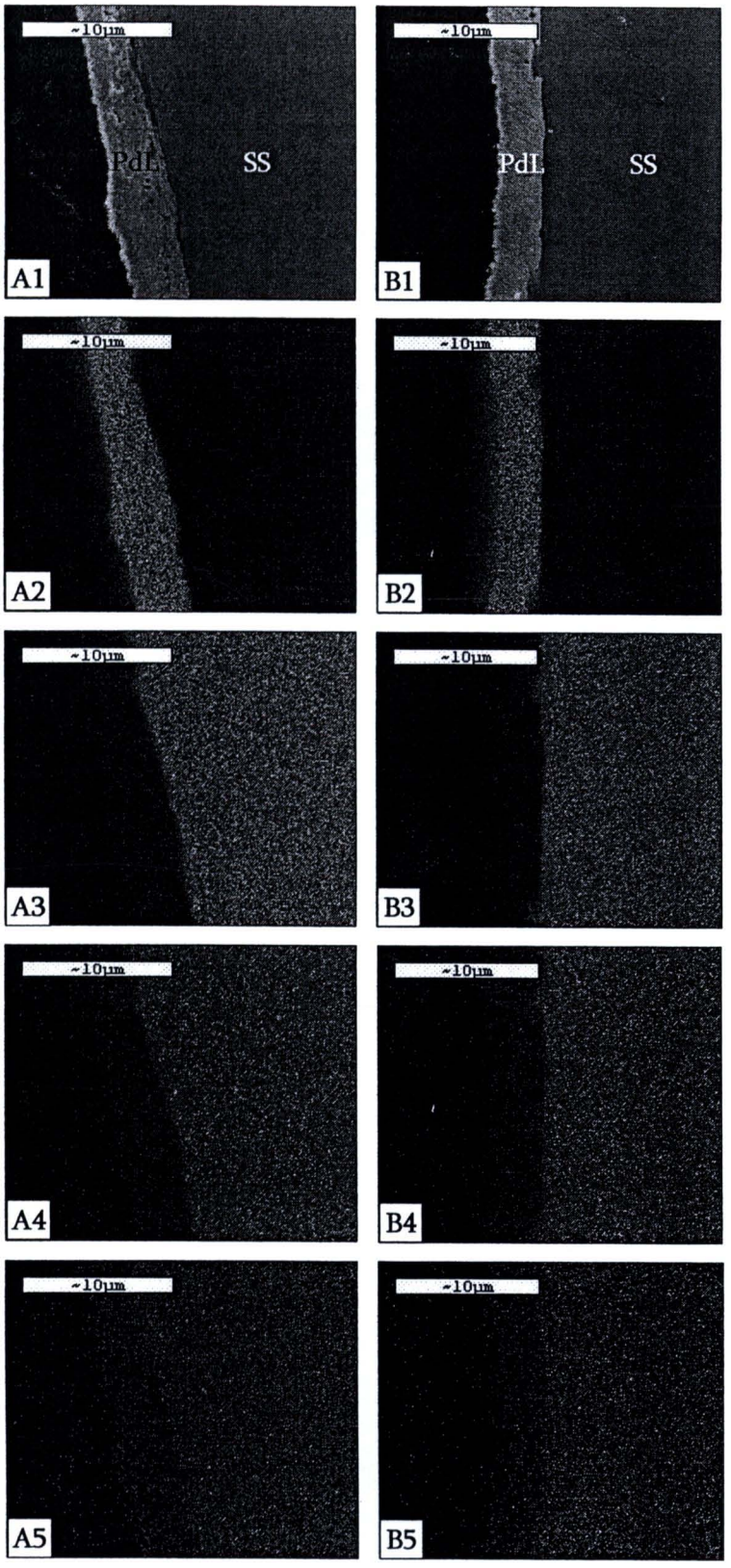

Figure 4.11 SEM micrographs (2500X) of the cross sections of palladium membrane after heating for 24 hr at 450°C. Column A (A1-A5): unoxidized, no barrier; B (B1-B5): Cr_2O_3 barrier by thermal oxidation. Metal distribution were mapped in each row: row 2 (A2-F2): Pd; 3 (A3-F3): Fe; 4 (A4-F4): Cr; and 5 (A5-F5): Ni. Arrow head: intermetallic diffusion barrier, PdL: Pd layer, SS: stainless steel.

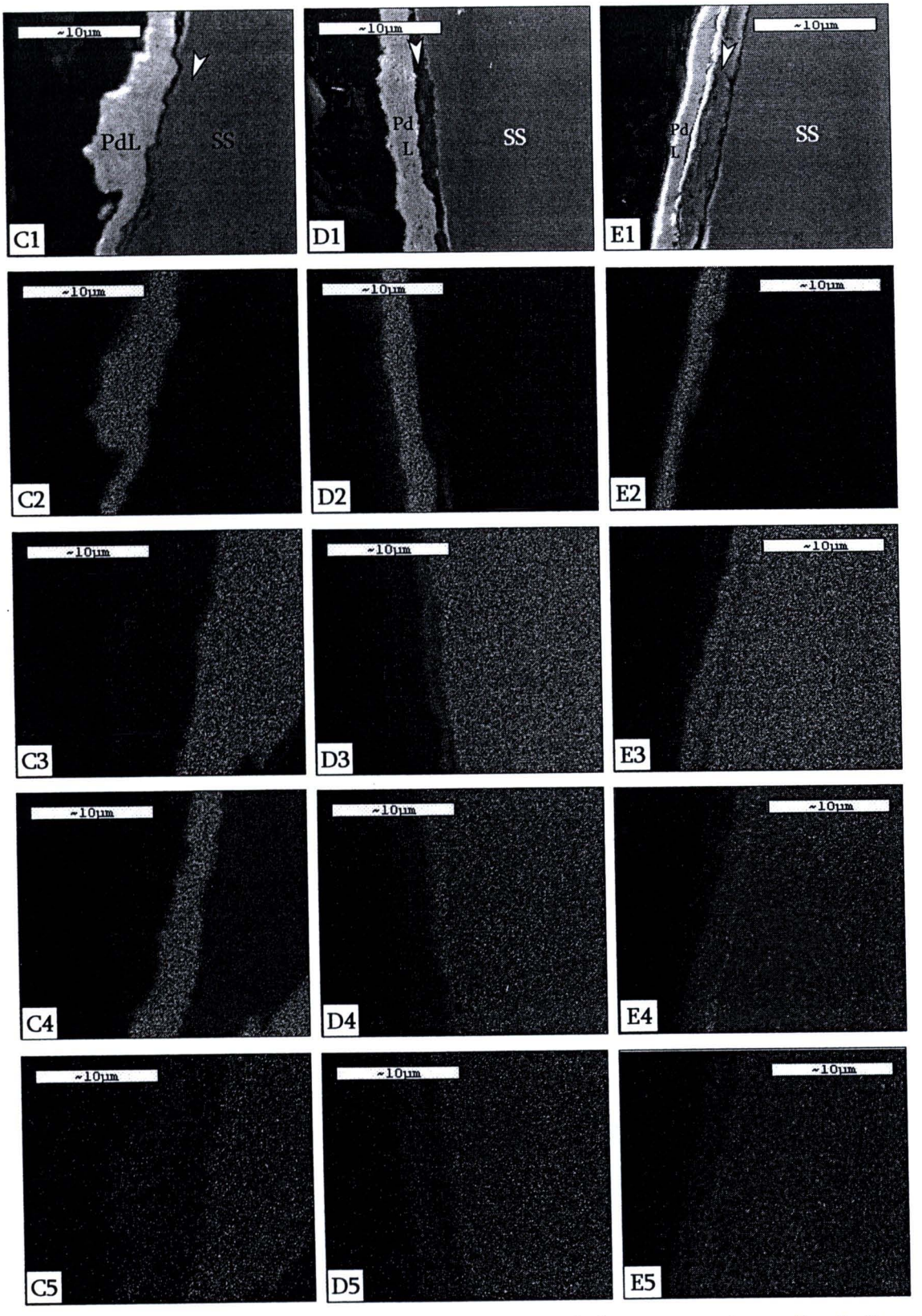

Figure 4.11 (continued) SEM micrographs (2500X) of the cross sections of palladium membrane after heating for 24 hr at 450°C. Column C (C1-C5): Cr_2O_3 barrier by Cr-electroplating/oxidation; D (D1-D5): Cr_2O_3 barrier by Cr-sputtering/oxidation; E (E1-E5): CrN barrier by sputtering. Metal distribution were mapped in each row: row 2 (A2-F2): Pd; 3 (A3-F3): Fe; 4 (A4-F4): Cr; and 5 (A5-F5): Ni. Arrow head: intermetallic diffusion barrier, PdL: Pd layer, SS: stainless steel.

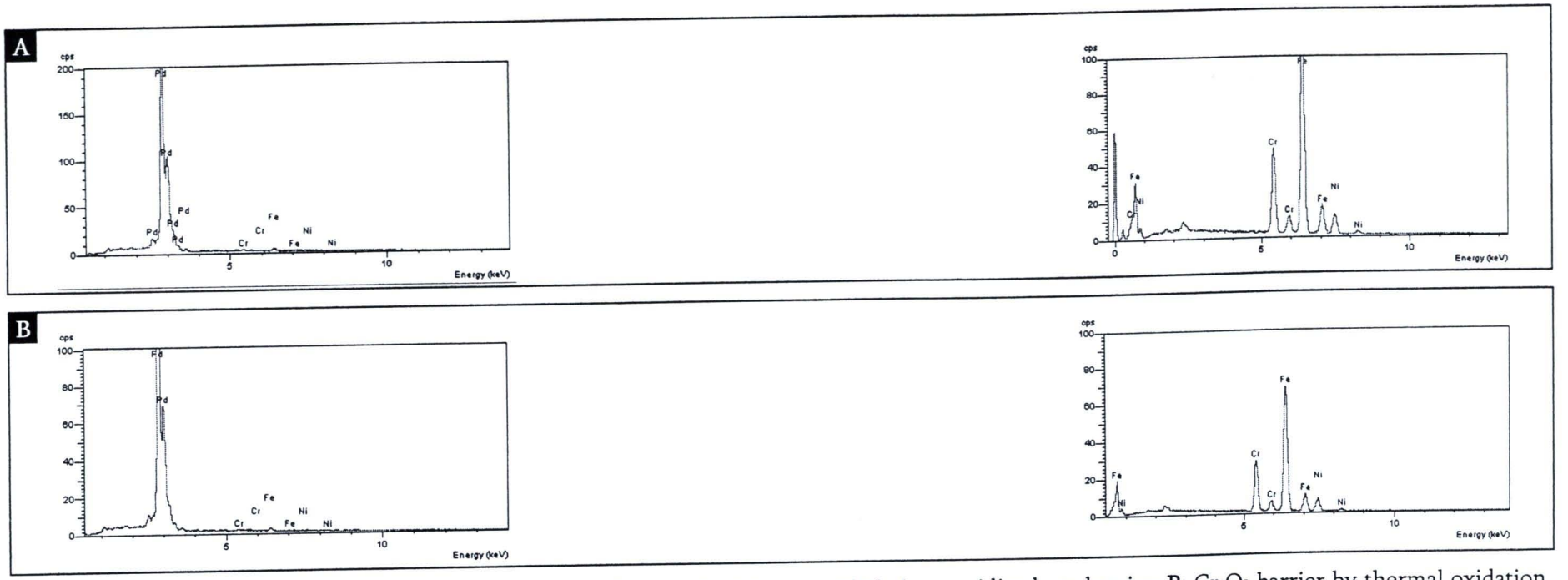

Figure 4.12 EDS spectra of the palladium membrane after heating for 24 hr at 450°C. A: unoxidized, no barrier; B: Cr_2O_3 barrier by thermal oxidation. EDS spectra of the Pd layer are shown on the left, those of the Cr-based intermetallic diffusion barrier are in the middle and those of the stainless steel support are on the right.

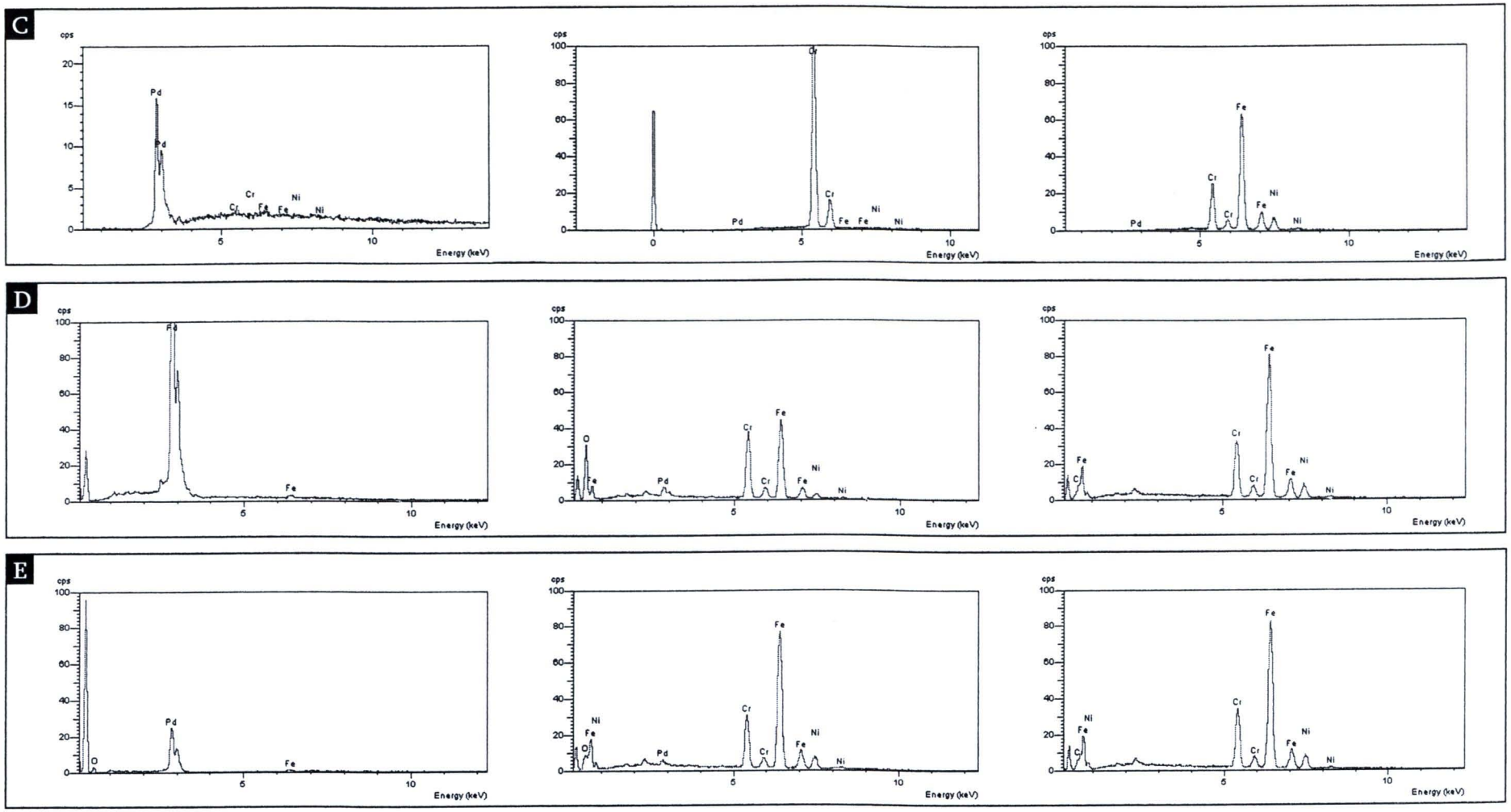

Figure 4.12 (continued) EDS spectra of the palladium membrane after heating for 24 hr at 450°C. C: Cr_2O_3 barrier by Cr-electroplating/oxidation; D: Cr_2O_3 barrier by Cr-sputtering/oxidation; E: CrN barrier by sputtering. EDS spectra of the Pd layer are shown on the left, those of the Cr-based intermetallic diffusion barrier are in the middle and those of the stainless steel support are on the right.

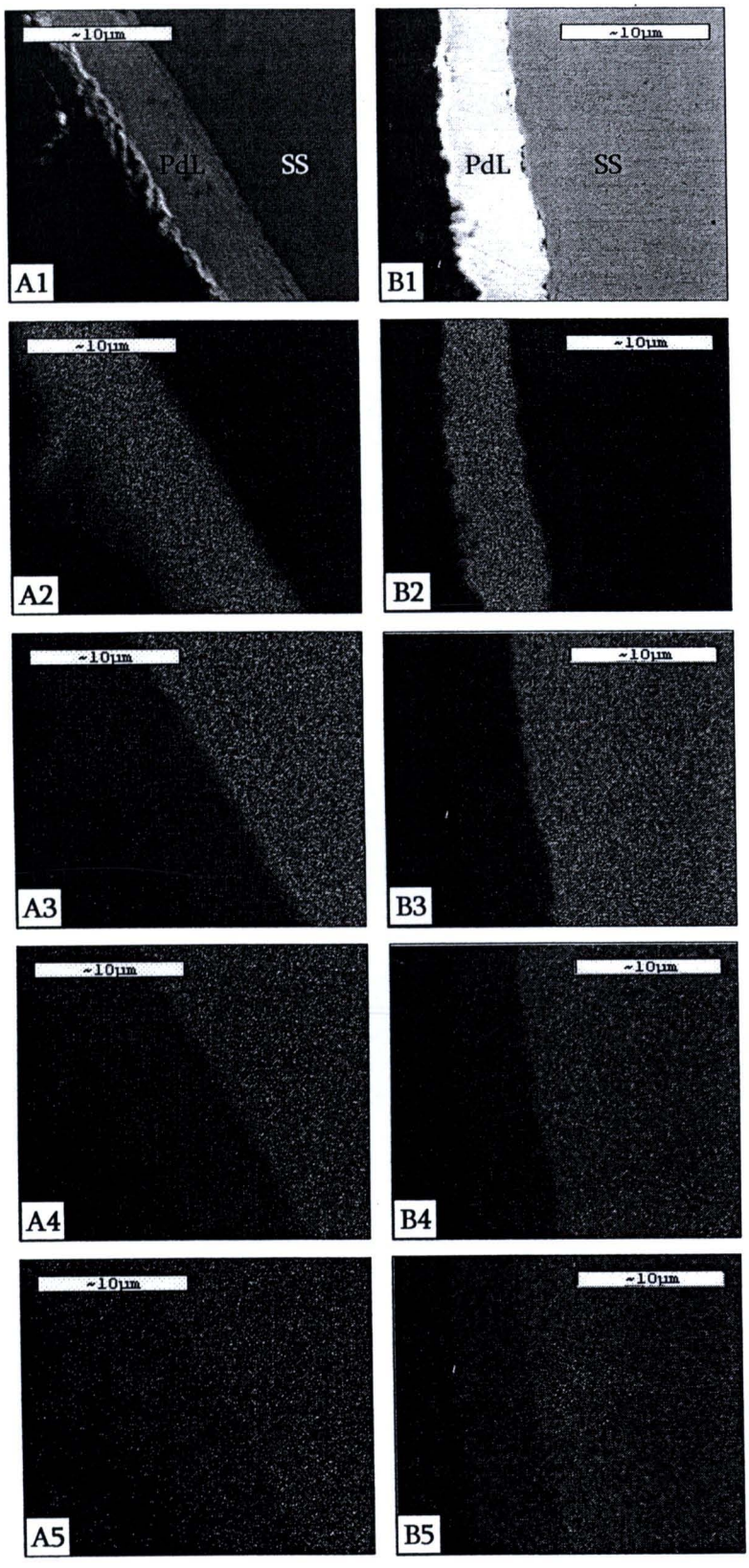

Figure 4.13 SEM micrographs (2500X) of the cross sections of palladium membrane after heating for 24 hr at 500°C. Column A (A1-A5): unoxidized, no barrier; B (B1-B5): Cr_2O_3 barrier by thermal oxidation. Metal distribution were mapped in each row: row 2 (A2-F2): Pd; 3 (A3-F3): Fe; 4 (A4-F4): Cr; and 5 (A5-F5): Ni. Arrow head: intermetallic diffusion barrier, PdL: Pd layer, SS: stainless steel.

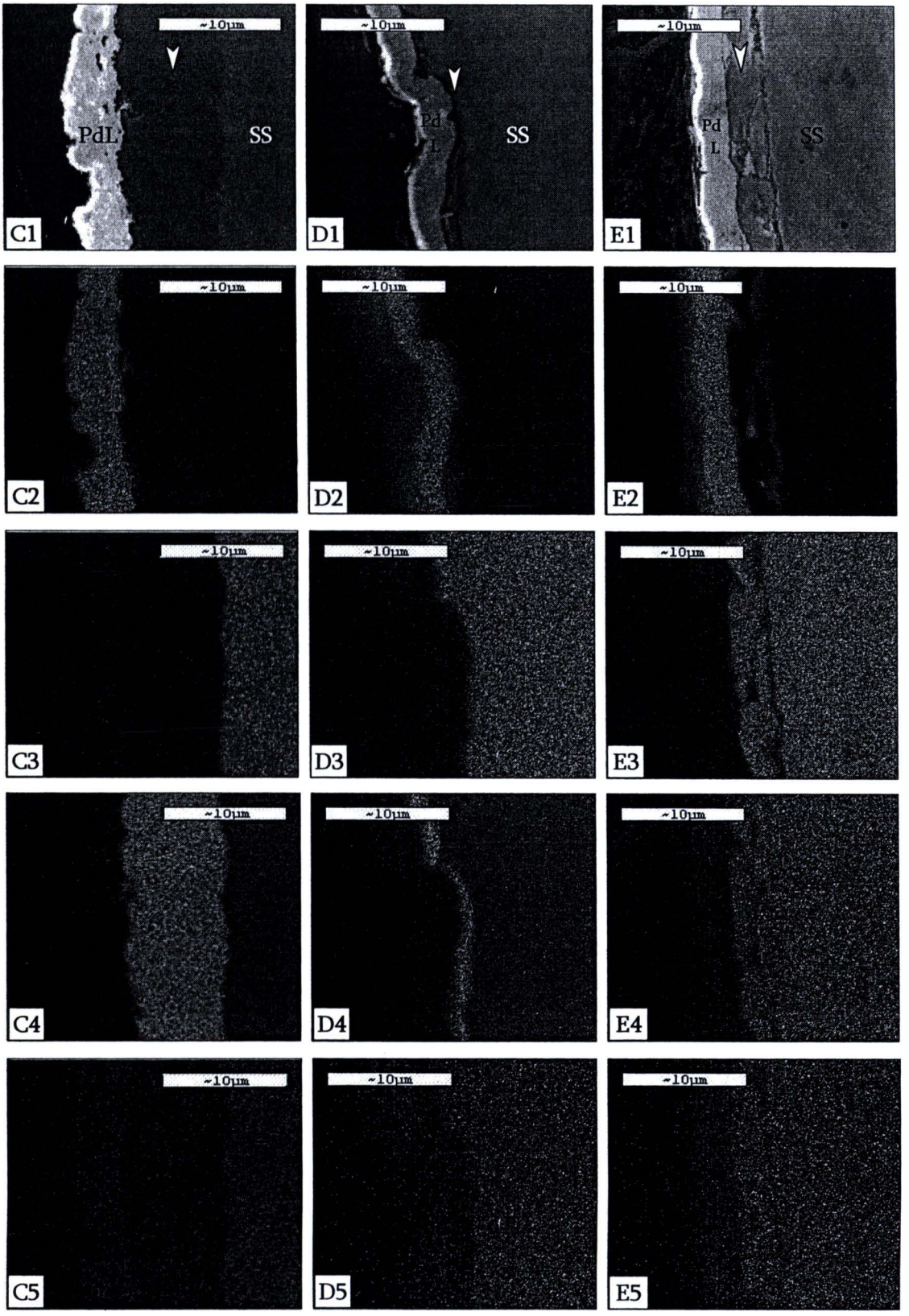

Figure 4.13 (continued) SEM micrographs (2500X) of the cross sections of palladium membrane after heating for 24 hr at 500°C. Column C (C1-C5): Cr_2O_3 barrier by Cr-electroplating/oxidation; D (D1-D5): Cr_2O_3 barrier by Cr-sputtering/oxidation; E (E1-E5): CrN barrier by sputtering. Metal distribution were mapped in each row: row 2 (A2-F2): Pd; 3 (A3-F3): Fe; 4 (A4-F4): Cr; and 5 (A5-F5): Ni. Arrow head: intermetallic diffusion barrier, **PdL**: Pd layer, **SS**: stainless steel.

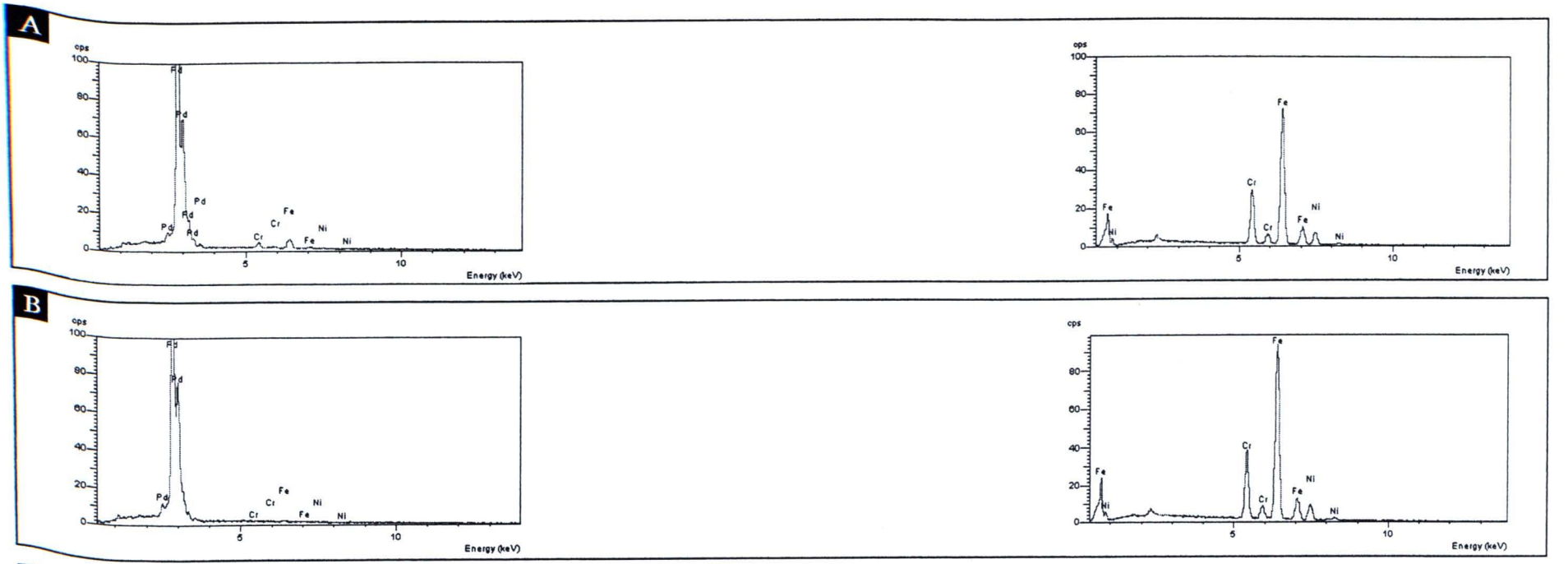

Figure 4.14 EDS spectra of the palladium membrane after heating for 24 hr at 500°C. A: unoxidized, no barrier; B: Cr_2O_3 barrier by thermal oxidation. EDS spectra of the Pd layer are shown on the left, those of the Cr-based intermetallic diffusion barrier are in the middle and those of the stainless steel support are on the right.

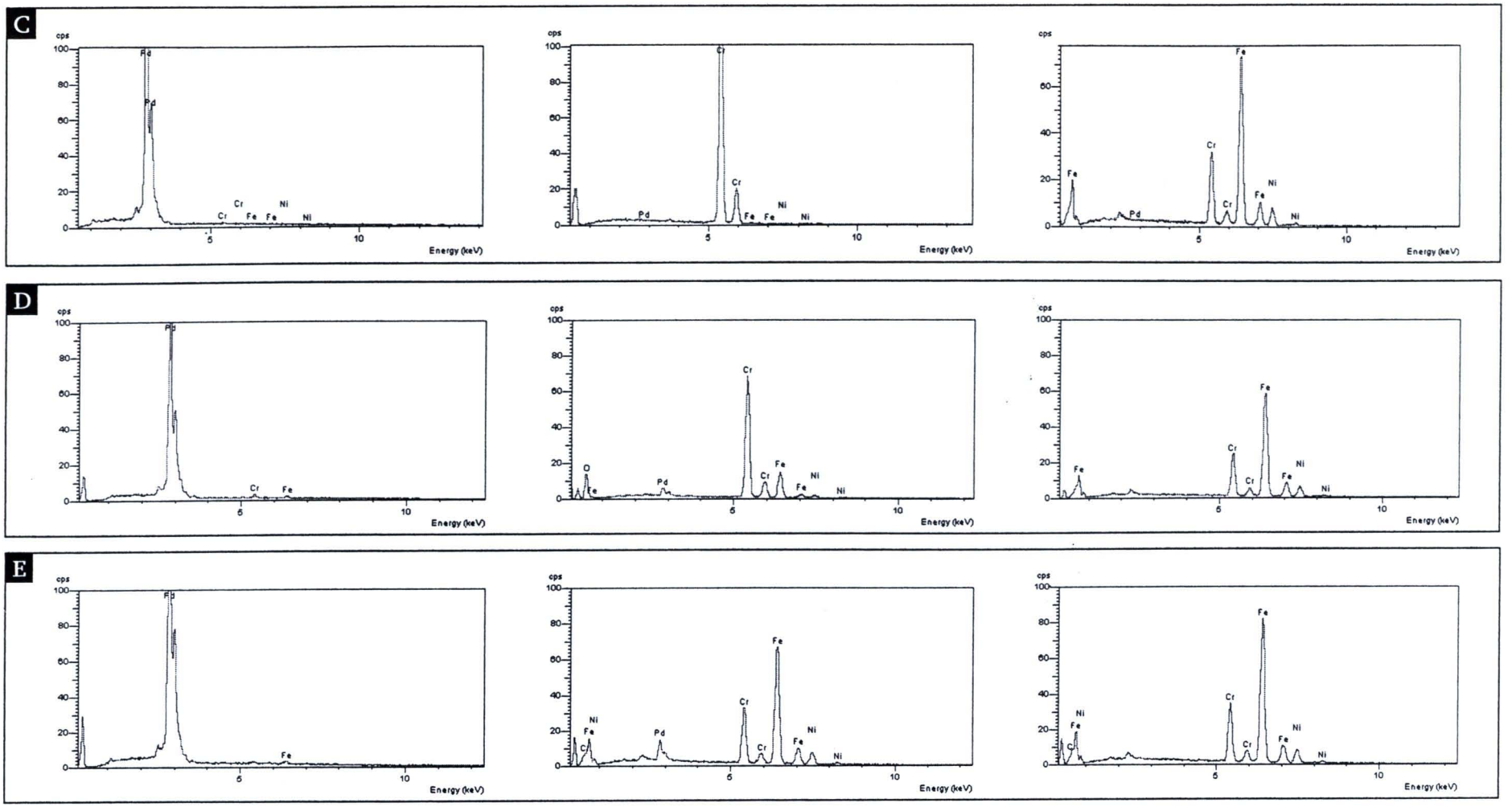

Figure 4.14 (continued) EDS spectra of the palladium membrane after heating for 24 hr at 500°C. C: Cr_2O_3 barrier by Cr-electroplating/oxidation; D: Cr_2O_3 barrier by Cr-sputtering/oxidation; E: CrN barrier by sputtering. EDS spectra of the Pd layer are shown on the left, those of the Cr-based intermetallic diffusion barrier are in the middle and those of the stainless steel support are on the right.

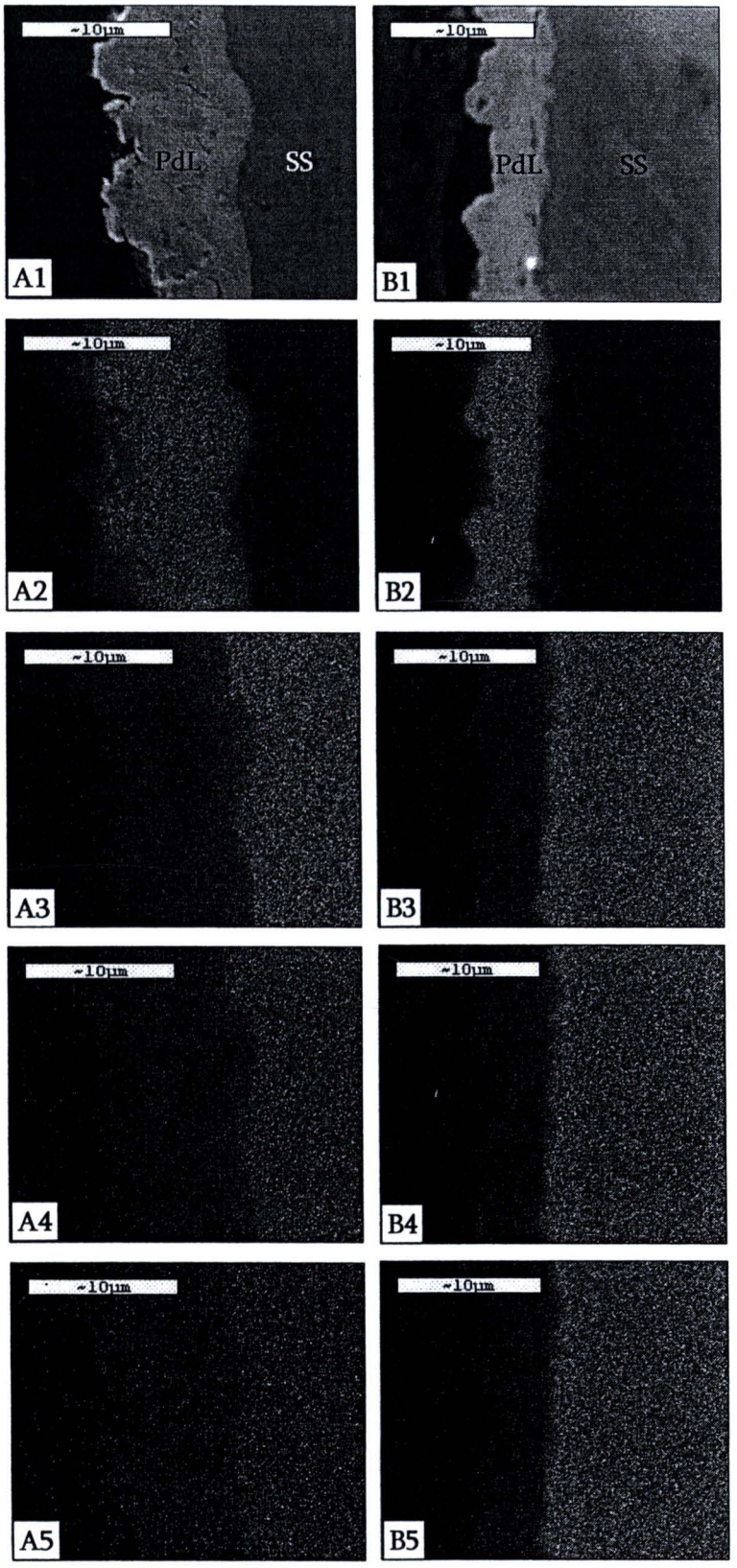

Figure 4.15 SEM micrographs (2500X) of the cross sections of palladium membrane after heating for 24 hr at 550°C. Column A (A1-A5): unoxidized, no barrier; B (B1-B5): Cr_2O_3 barrier by thermal oxidation. Metal distribution were mapped in each row: row 2 (A2-F2): Pd; 3 (A3-F3): Fe; 4 (A4-F4): Cr; and 5 (A5-F5): Ni. Arrow head: intermetallic diffusion barrier, PdL: Pd layer, SS: stainless steel.

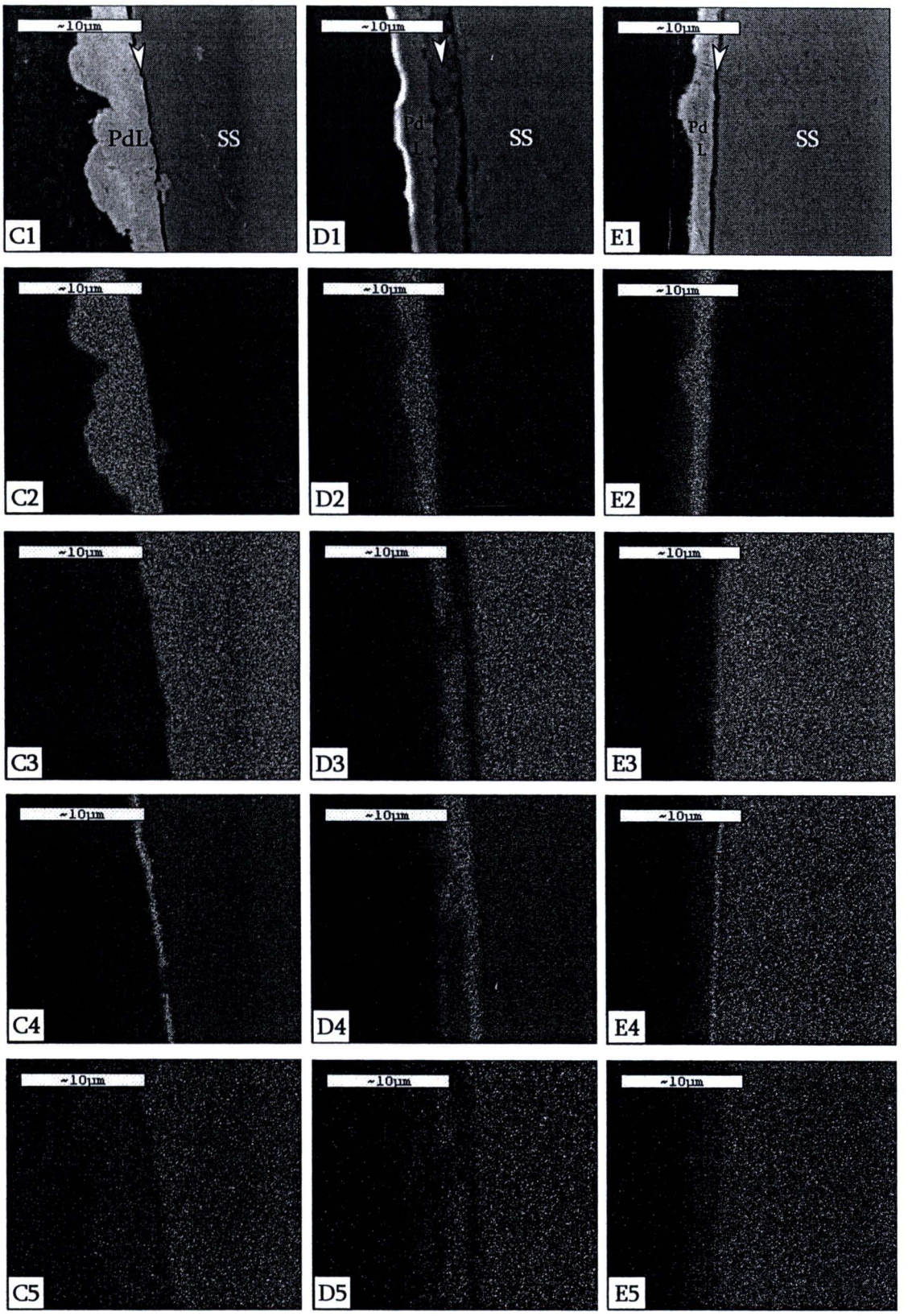

Figure 4.15 (continued) SEM micrographs (2500X) of the cross sections of palladium membrane after heating for 24 hr at 550°C. Column C (C1-C5): Cr_2O_3 barrier by Cr-electroplating/oxidation; D (D1-D5): Cr_2O_3 barrier by Cr-sputtering/oxidation; E (E1-E5): CrN barrier by sputtering. Metal distribution were mapped in each row: row 2 (A2-F2): Pd; 3 (A3-F3): Fe; 4 (A4-F4): Cr; and 5 (A5-F5): Ni. Arrow head: intermetallic diffusion barrier, **PdL**: Pd layer, **SS**: stainless steel.

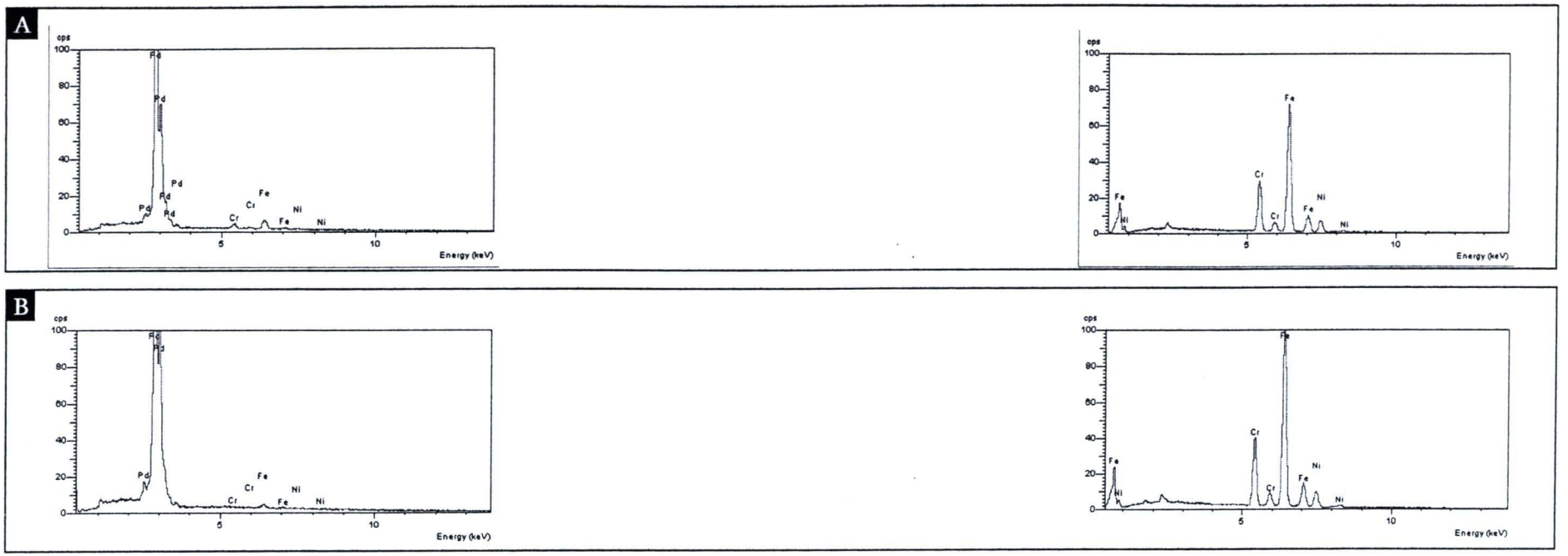

Figure 4.16 EDS spectra of the palladium membrane after heating for 24 hr at 550°C. **A**: unoxidized, no barrier; **B**: Cr_2O_3 barrier by thermal oxidation. EDS spectra of the Pd layer are shown on the left, those of the Cr-based intermetallic diffusion barrier are in the middle and those of the stainless steel support are on the right.

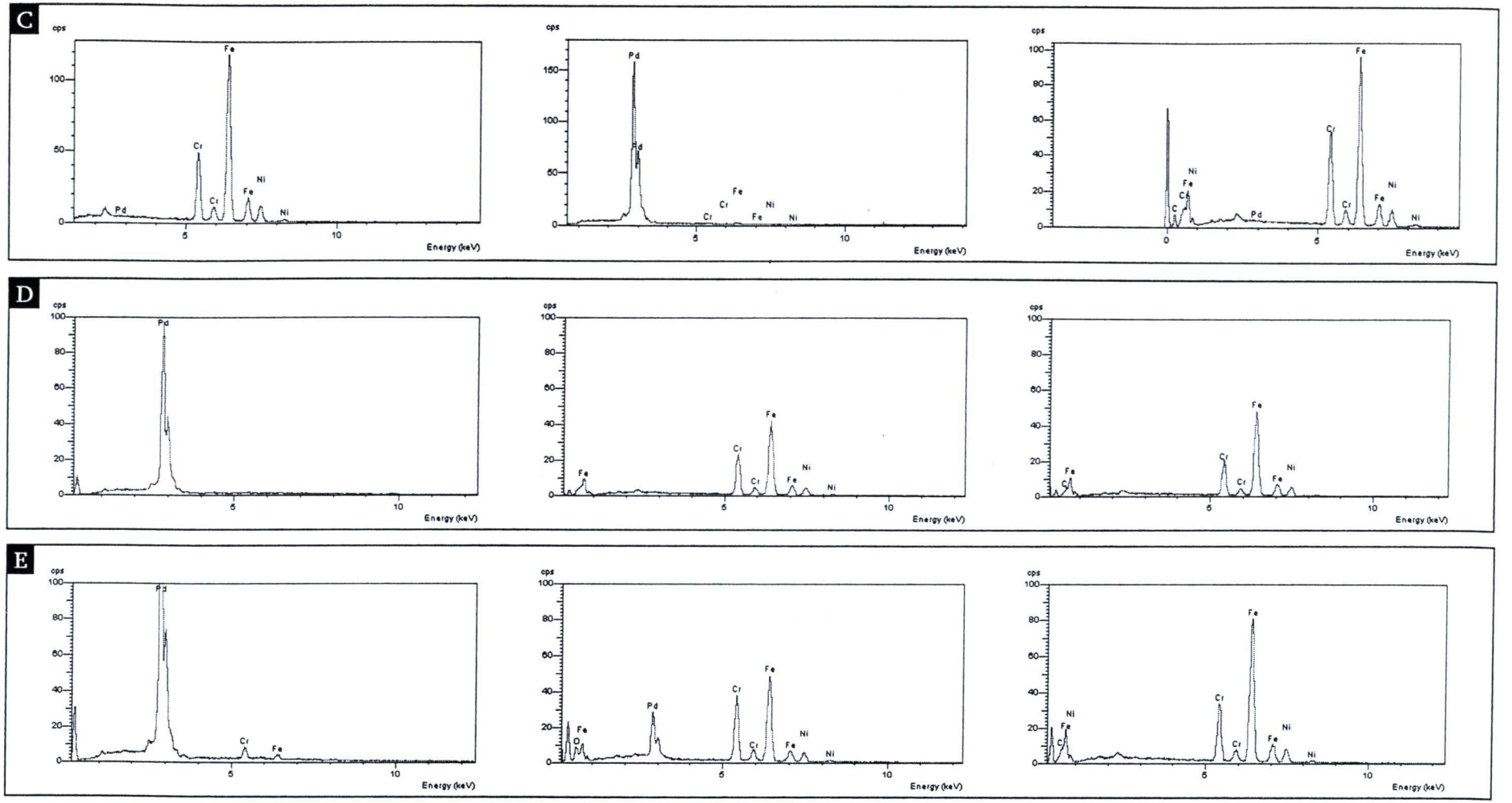

Figure 4.16 (continued) EDS spectra of the palladium membrane after heating for 24 hr at 550°C. C: Cr_2O_3 barrier by Cr-electroplating/oxidation; D: Cr_2O_3 barrier by Cr-sputtering/oxidation; E: CrN barrier by sputtering. EDS spectra of the Pd layer are shown on the left, those of the Cr-based intermetallic diffusion barrier are in the middle and those of the stainless steel support are on the right.

4.5 Effects of intermetallic diffusion barriers on palladium membrane morphology

The palladium layers were also melted at 500 and 550°C as revealed in Figure 4.9 by changed surface morphologies. Very little change was found at 450°C. Its trend, however, was not consistent with one another when compare with other types of support. In one case, the surface showed clumps of palladium and larger grain size but in the other meting results in finer, more even surface.

The explanations for such inconsistency do not lie in the palladium layer itself but the surface that supports them. Intermetallic diffusion barriers, to different degrees, influence how palladium atoms deposit on its support. Without doubt, different surface textures resulted in different palladium layer morphologies: smoother support surface resulted in finer, more even palladium layer surface (compare Figure 4.16IA, IB and IC). However, the chemical nature of the support surface does no small part in directing palladium membrane morphology. When compare among the finest support surfaces, i.e. the unoxidized, the Cr_2O_3-coated by oxidized Cr-sputtering and the CrN-coated, no one expects that the palladium layer was on a support of comparable level of fineness if they use the surface texture as a sole criterion.

My point in discussing this issue is not to explain why or how the two mentioned factors exert theirs influence on palladium layer morphologies. It just serves the purpose of reminding you that an effective intermetallic diffusion barrier cannot be judged alone in term of its efficacy in shielding the palladium layer. The question, Is the palladium layer still highly selective for hydrogen gas if its morphology is altered by the barrier, should be always ranked at the first place. The best intermetallic diffusion barrier in term of shielding the palladium layer could make the membrane itself the worst in term of selectivity for hydrogen gas and hence useless.

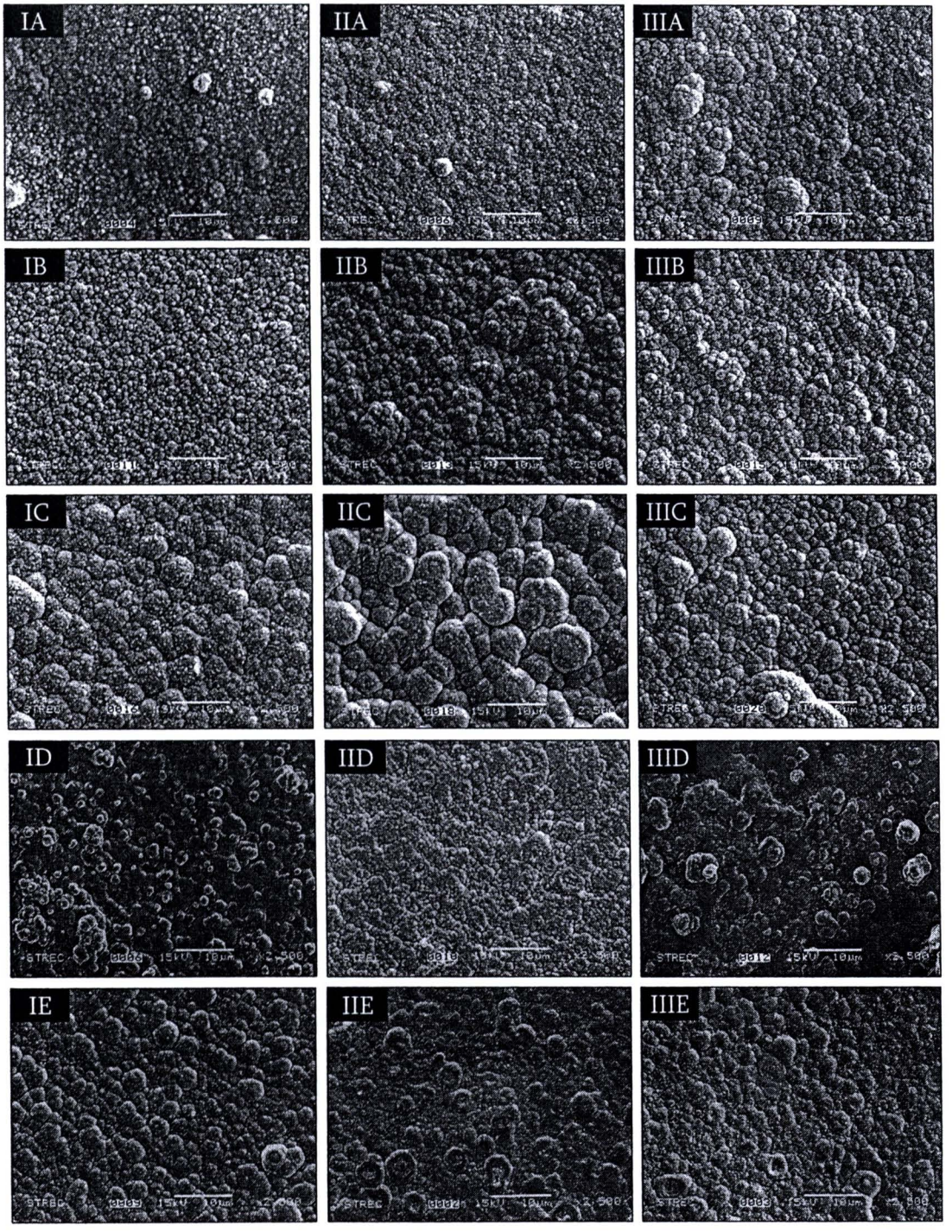

Figure 4.17 SEM micrographs (2500X) of the surface of the palladium layer on different intermetallic diffusion barrier after heating for 24 hr at 450°C (column I, IA-IE), 500°C (column II, IIA-IIE) or 550°C (column III, IIIA-IIIE). Row A (IA-IIIA): unoxidized, no barrier; B (IB-IIIB): Cr_2O_3 barrier by thermal oxidation; C (IC-IIIC): Cr_2O_3 barrier by Cr-electroplating/oxidation; D (ID-IIID): Cr_2O_3 barrier by Cr-sputtering/oxidation; E (IE-IIIE): CrN barrier by sputtering.